COMPOSITION OF THE MOON AS DETERMINED FROM ORBIT BY GAMMA-RAY SPECTROSCOPY

by

Albert E. Metzger

Space Sciences Division, Jet Propulsion Laboratory, Pasadena, CA 91109

Prepared for: Remote Geochemical Analysis (C. Pieters and P. Englert, Eds.)
to be published by the Lunar and Planetary Institute, Houston

Submitted: 6-20-90

Revised: 1-22-91

INTRODUCTION

A spacecraft placed in a planetary orbit of suitably high inclination will pass over all or most of the planet's surface in a matter of several weeks to months. The quite prodigious scientific potential of planetary orbiters lies in coupling this comprehensive coverage with observing systems capable of gathering data on properties that include elemental and mineralogic composition, exogenic and endogenic surface alterations, thermal balance, gravity, topography, stratigraphy, albedo and magnetism. Observations made from the orbiter are capable of characterizing the body as a whole, as well as specific regions, at a level of spatial detail dependent on the resolution of the observing instrument. For a gamma-ray spectrometer, repeated traverses are necessary in order to build up sufficient counting statistics within the field of view. When this has been accomplished, areas found to be of special interest can be identified for more intensive investigation by other orbiting experiments or as candidate sites for landed missions capable of more detailed examination.

Gamma-ray spectroscopy from lunar orbit directly addresses the chemical composition of the surface and, indirectly, what that knowledge signifies about the origin, evolution, and present state of the Moon. The Moon's surface composition is the end product of a series of processes beginning with condensation of the nebula and proceeding through stages of accumulation, collision and modification. Extensive heating following gravitational impact during accretion lead to chemical differentiation and the formation of a crust, a mantle and perhaps a core.

The naturally radioactive elements K, U, and Th, produce heat as they decay. Given sufficient concentrations of these elements, over a long period of time this heat will melt the rocks in which they are dispersed. When melting occurs, as in the Earth, the radioactive elements are among those fractionated in the process and enriched near the surface of the body. They are thus a cause, together with the energy generated by gravitational accretion, of planetary heating as well as a manifestation of its consequence, The abundance of K, U and Th in the lunar surface can be determined by measuring the gamma rays produced as they decay. Other elements in the surface, upon irradiation by energetic cosmic rays, undergo reactions that are accompanied by the emission of characteristic gamma rays. The energy of these gamma rays identifies the emitting element, while their intensity is proportional to concentration. The absence of an absorbing lunar atmosphere makes it possible to record lunar gamma rays at orbital altitudes. A discussion on the production of characteristic gamma rays by radioactive decay and by cosmic-ray excitation can be found in the chapter by Evans, Reedy and Trombka.

The possibility of performing a remote gamma-ray spectroscopy experiment at the Moon as a means of determining the composition of its surface was discussed by several individuals in the 1950's, most productively by Arnold (1958), His proposal led to the first attempt to perform such an experiment, an effort to obtain information superior to the then state of knowledge which is illustrated in Fig. 1.

Following two test flights to initiate the Ranger lunar program, the Ranger 3, 4, and 5 spacecraft were launched in an effort to hard land a seismometer on the Moon's surface and, in the final minutes of a direct trajectory, to obtain pictures and measure the gamma-ray flux. The gamma-ray spectrometer on board consisted of a CSI (Tl) scintillation detector in the form of a right circular cylinder 70 mm in length and in diameter, enclosed within a plastic scintillator 3 mm thick (Van Dills et al., 1962). The latter served as a phoswich type of anticoincidence shield for the purpose of rejecting events due to the passage of cosmic-ray particles through the detector (Evans et al. , this book). Thirty-two channels of pulse height analysis were provided by the electronics. The nominal gain range was set at O-3 MeV, with provision for a commanded change to 0-0,6 MeV. Instrument energy resolution, defined as the full energy width at half-maximum amplitude of the Cs-137 0.662 MeV gamma ray photopeak, ranged from 11.% to 13.5%. Inflight calibration was provided by a source of low energy gamma-ray lines. The detector was positioned at the end of a two meter telescopic boom. Separation from the spacecraft reduced the level of background interference due to gamma rays produced by cosmic-ray reactions with materials of the spacecraft. The electronics were mounted on the main

frame. Astronomical data was obtained in cislunar space, namely, the first measurement of the diffuse cosmic gamma-ray flux in the MeV range (Metzger et al., 1964), but spacecraft trajectory and power problems voided the lunar objective.

The first instrument to record identifiable gamma rays from the Moon was carried on the U.S.S.R. Luna 10 mission in 1966 (Vinogradov et al., 1.968) . With thirty-two channels of pulse height analysis, a 30 mm by 40 mm NaI (Tl) scintillation crystal, and the phoswich type of charged particle rejection system, the Luna 10 instrument resembled that on the Ranger spacecraft. However, the small size of the crystal provided a response efficiency less than one-fifth as great, and its location on the main frame of the spacecraft imposed a substantially higher proportion of background interference.

Nine pulse height spectra were obtained by the Luna 10 gamma-ray spectrometer, seven over an energy range from O-3 MeV, two from 0-0.6 MeV. In addition, thirty-nine measurements of the integrated response from 0.3-0.7 MeV were recorded over various lunar locations at mean spacecraft altitudes ranging from 400 to 1,000 km. The preponderance of continuum gamma-ray radiation over the lunar chemical signature was noted, but the first order fact that the lunar highlands are not granitic in composition was clearly established. Comparison of the thirty-nine integrated 0.3-0.7 MeV measurements showed the lunar component to be 15-20% greater over mare regions than over highland regions (Vinogradov et al., 1968). However, comparison with subsequent Apollo data from corresponding locations shows little correlation.

In 1967 and 1968, three measurements of lunar surface composition were made by alpha backscattering instruments on the Surveyor 5, 6, and 7 landed spacecraft (Patterson et al., 1969). Two locations were in mare areas, the third was in the highlands. Concentrations of eight elements were reported. The mare compositions were found to be similar and, apart from having higher titanium and lower sodium content, comparable to the composition of terrestrial ocean ridge basalts (Turkevich, 1971). Surveyor 7 landed near the crater Tycho and identified major differences between maria and highland composition, the latter having smaller amounts of titanium and iron, as well as larger amounts of aluminum and calcium.

In 1969, the Apollo 11 mission returned the first samples from the Moon. In 1972 and 1973, Apollo 15 and Apollo 16 carried into lunar orbit a complement of instruments, one of which was a gamma-ray spectrometer. The remainder of this chapter will focus on the Apollo 15 and Apollo 16 gamma-ray observations and their significance.

THE APOLLO INSTRUMENT AND ITS PERFORMANCE

The Apollo gamma-ray spectrometer (AGRS) is briefly described by Evans et al. (this book); for additional details see Barrington et al. (1974). The instrument was mounted on the end of a boom measuring 7.6 meters when fully extended, but which was capable of being placed at intermediate positions by astronaut timing control for the purpose of separating and subtracting the spacecraft background component. No useful data was

obtained prior to descent of the lunar module, due to the local production of gamma rays by a radioisotopic thermoelectric generator which was present as the power source for the Apollo surface experiment package. After lunar module separation, the data-taking duty cycle for the remaining approximately 50 lunar orbits was as high as the mission sequence plan permitted, Data taken during the return trip to Earth provided background and astrophysical information. The nearly circular orbits of Apollo 15 and 16 ranged from 100 to 1.20 kilometers above the surface. At this altitude the spatial resolution, defined as the radial distance at which the flux from a point source drops to one-half of its intensity at the nadir (Figure 3 in Evans et al., this book), is about 75 km.

The orbit of Apollo 15 was inclined at 30° to the equator, that of Apollo 16 was nearly equatorial at 9°. Combined coverage during useful data-taking periods amounted to 23% of the lunar surface, none of it at latitudes greater than 30°. Spacecraft maneuvers and a small amount of orbit-to-orbit precession broadened the ground track. Variations in the amount of observing time-per unit area were often large, particularly at the edges of the Apollo 15 track. Areas measured from both Apollo 15 and 1.6 have been very useful as a cross-check and as a means of normalizing the two data sets.

A Hg-203 calibration source of 0.279 MeV gamma rays augmented the 0.511 MeV positron line and major compositional lines for tracking the stability of the instrument. The Apollo 15 AGRS underwent a 27% loss in gain and a zero offset drift of several. tenths of a charnel., most of it during the first half of the period in lunar orbit, This was traced to photomultiplier

tube aging. The Apollo 16 AGRS was preconditioned and showed only an 8% gain fluctuation and no measurable zero offset drift. Energy resolution in flight was 8.6% for the Apollo 15 instrument, and 7.4% for the Apollo 16 instrument, both much superior to the Ranger instruments; the Apollo 16 value in particular was comparable to a fine laboratory system of the period.

Seventy-four hours of Apollo 15 data were collected in lunar orbit with the boom fully extended. Not all of this was recovered from the ground stations. Applying the additional selection criteria requiring an unobstructed view of the Moon, the nominal gain step setting, anticoincidence shield operation, and orbit-to-orbit consistency (Metzger et al., 1977), the quality data base for Apollo 15 totaled 36.3 hr below 2.75 MeV, 40.6 hr above 2.75 MeV, and 41.0 hours for Apollo 16. In terms of the combined ground track this amounts to an average of 12.6 min. per $5° \times 5°$ pixel of latitude and longitude. The actual observing times over areas of this size ranged from a few seconds to 0.6 hour.

The nominal energy range of analysis to which the Apollo instrument was set, 0.2-10 MeV. spans nearly all useful gamma-ray lines from surface material. Analog signals from the detector were translated into 511 channels of uniform energy intervals, plus an additional channel for gamma rays of energy above the maximum incremental value. The output data was transmitted as a bit-serial data stream on an event-by-event basis. The data was grouped into words of ten bits per gamma-ray event, and these words were in turn arranged into frames of 128 words. The first seven words of each frame were devoted to a pre-established synchronization code, followed

by the status of the anti-coincidence signal and the contents of three single channel accumulators, one of which measured instrument live time. Each of the remaining 121 words conveyed gamma-ray spectral information if an event was present in the output register at the time of readout. Nine of the bits within each word represented the number of gated-clock pulses accumulated in the gated-clock counter, corresponding to the registered amplitude of the gamma-ray event. The tenth bit was inserted by the parity generator in order to check for errors in the data transmission.

DATA REDUCTION

General

Transmission of the data on an event-by-event basis as described above preserved spatial resolution and permitted complete flexibility in binning the data according to any desired arrangement of time or spacecraft location. Translating the accumulated pulse height spectra to elemental concentrations is complex, requiring a knowledge of the relevant background components , the response of the instrument, the observing geometry, and the production of gamma rays per unit surface concentration (Evans et al., this volume) .

The lunar spectrum consists of a discrete line component which contains the compositional information, together with a continuum. Because of its strength and the degree to which the limited energy resolution of the NaI detector broadens the incident gamma-ray lines, the continuum dominates the

spectrum, contributing about 85 percent of the response, the precise proportion varying with energy and surface composition. The continuum is predominantly generated by secondary processes following the interaction of cosmic rays with the lunar surface, principally the electron-positron cascade and multiplication, together with electron bremsstrahlung and multiple scattering. A portion of the discrete emission also undergoes Compton scattering in the lunar surface and adds to the continuum. Figure 2 shows a lunar pulse height spectrum before and after its separation into continuum and discrete line components (see also Table 4 of Evans et al.. , this book) . Three methods have been employed to derive surface concentrations from the latter, response function analysis, energy band analysis, and photopeak analysis. Each will be discussed in turn.

F2

Response Function Analysis

The response of a detector to an incident gamma ray is dictated by the three interaction mechanisms, photopeak absorption, Compton scattering, and pair production (Evans et al. , this book), whose relative effectiveness depends on the size, shape , and material of the detector as well as the energy of the gamma ray. Individual response functions correspond to monoenergetic gamma rays. A set or library of response functions specific to the NaI scintillator in the Apollo gamma-ray spectrometer was obtained by measurements with standard gamma-ray sources and Monte Carlo calculations (Berger and Seltzer, 1972). From one to several gamma rays may contribute significant emission from a particular element. Individual response functions corresponding to monoenergetic gamma rays can be added in proportion to their relative intensity to produce a spectrum characteristic

of emission from a particular element (Trombka et al. , 1979). A set of these monoelemental response functions of most interest to the Apollo analysis is shown in Fig. 3. In addition to the photopeak, gamma rays above 1 MeV undergo pair production leading to first and second escape peaks which become significant spectral features for gamma rays above 3 MeV. The complexity of the composite discrete spectrum shown as the top line of Fig. 3, and the small photopeak to Compton scattering ratio of most of the lines, suggests use of the entire monoelemental response function to characterize a particular element rather than confining the analysis to the area of the photopeaks. As used, the technique applies a least squares fit of selected library response functions covering the energy range of the measurements to the measured data (Trombka and Schmadebeck, 1968) . The library of monoenergetic response functions is also used to obtain an estimate of the continuum spectrum. This continuum is then subtracted from the original spectrum to give a first estimate of the total discrete line spectrum. The library of monoelemental response functions is fitted to the discrete line spectrum by means of a matrix inversion analysis Subtracting the total discrete line spectrum from the original spectrum gives a second estimate of the continuum. The process is repeated until a good fit is obtained for both the continuum and the monoelemental response functions. Typically this has required about three iterations. A comparison between the top curve of Fig. 3 and the crosses which correspond to the separated discrete line spectrum shows the fit between the combined response functions and the corresponding composite lunar spectrum. A transformation from observed counts to emitted photons and application of the estimated rates of production yields values of concentration.

In application, a nine component response function library was used which included elements like Ca and Al from which no useful data has been obtained (Metzger et al. , 1974). To reduce the number of variables, Th and u were combined into a single component with an abundance ratio of 3.8, the commonly observed value in lunar rocks and soils. Thorium concentrations were obtained by applying this ratio to the resultant value of the total component. Although well determined in the analysis, Si and O values were fixed based on returned sample analyses because their variation over the lunar surface is less than the uncertainty of their determination here. The continuum was separated into two components, one due to cosmic-ray cascade processes and independent of count-rate, the other due to Compton scattering of gamma rays from natural radioactivity in the lunar surface, which varies with the count rate and predominates at lower energies (Bielefeld et al., 1976) . Element concentrations are sensitive to the selection of the continuum, hence the need to iterate stated above. Normalization factors based on the results of returned Apollo sample analyses were needed for those elements whose gamma-ray lines are the result of cosmic-ray interactions , for which accurate knowledge of the production parameters is limited. For the natural radioactivities (K and Th + U), the use of nuclear data and laboratory calibrations were found to be sufficient without the application of ground truth factors.

Energy Band Analysis

From the start of the Apollo gamma-ray data analysis, variations in lunar surface composition have been identified by accumulating the counting rate within given energy intervals over specified lunar surface areas

(Metzger et al., 1973). The most useful interval has been from 0,55 to 2.75 MeV. In the energy region above the positron line at 0.51 MeV (the line itself contains little chemical information), up to and including the highest energy line due to natural radioactivity, the 2.61 MeV Th line, the regional differences in count rate are predominantly due to varying concentrations of the radioactive elements Th, U, and K. This is a fortunate circumstance, since the statistical precision of the total count rate in this region is excellent, and the best possible areal resolution can thereby be obtained. With this sensitivity it has been possible to calculate the relative abundance of natural radioactivity for regions containing less than a minute of observing time.

Put in general terms, the energy band analysis technique analyzes a particular element through variations in count rate over specific portions of the energy spectrum where its effect is greatest. Composition can be obtained by matching a set of net lunar count rates with known surface concentrations . A regression line is defined by the relationship. The perturbing effect of other elements on the band count rate must be evaluated and removed if significant. With the response function method, a simultaneous analysis for many elements is performed by transforming the entire pulse height spectrum into an incident photon spectrum based on a library of component response functions. By comparison, energy band analysis employs the integrated count rate over limited energy intervals, does not require separation of the lunar spectrum into line and continuum components, yields results for one element at a time, and can be applied to shorter periods of observation.

Photopeak Analysis

The third method applied to derive concentrations from the AGRS data, photopeak analysis, used the matrix inversion of a set of functions for the purpose of fitting the approximately Gaussian photopeak response of the detector to an incident line flux. In this method the analysis is confined to a limited energy range within which one to several elements of interest have photopeaks or escape peak features. The analytic model used to describe the spectral data includes the contributions of photopeaks and/or escape peaks, the continuum and a linear background. This particular form of photopeak analysis can be applied to several elements at a time and to several peaks produced by the same element, is less dependent on an accurate isolation of the continuum component than library function analysis, but uses less of the information contained in the spectum. Photopeak analysis has seen only limited application to the Apollo gamma-ray data set.

Spatial Deconvolution

The Apollo gamma-ray spectrometer had a nearly isotropic response to lunar gamma radiation. Although this wide field of view was desirable in order to increase the intensity of the lunar signal, it penalized spatial resolution. As spatial resolution worsens, the boundaries between chemical provinces become increasingly diffuse, thereby limiting their definition, and chemical contrast is subdued. Accordingly, a method of deconvolving the instrument response was developed to partially restore spatial resolution and contrast by removing the smoothing effect of the detector (Haines et al., 1978). It has been successfully applied to Th, whose wide band signal

is strong enough to sacrifice some of the precision in the measurement of concentration in exchange for a significant improvement in spatial resolution and accuracy.

A 2° x 2° pixel array of concentrations and associated uncertainties derived from energy band analysis was assembled to define the data field. Concentrations observed at any location in orbit are the average of all concentrations within the field of view weighted by the geometry of response. A succession of geometric models of the regional surface concentration are convolved through the response function of the instrument. These models are developed by the most appropriate choices from a set of geometric constructs. Each construct defines or modifies a feature or boundary of the Th distribution on the lunar surface. For example, a "flat" construct gives every pixel in the model field a unit value. The "border" construct places a great circle arc through the model field. All pixels whose centers are on one side of the border are given unit value, those on the other side zero value, and so forth.

The predicted data field produced by the convolution integration is compared with that actually observed from orbit on a pixel by pixel basis using least squares analysis. Differences outside of statistical expectation are interpreted in terms of deficiencies in the model. Based on the comparison, the geometric model is improved; the improved model is convolved again and the least-squares analysis repeated until the quality of fit cannot be improved. Such forward iteration leads to models that are close to the Th distribution on the lunar surface. In practice, other considerations such as reasonableness of regional concentrations and

locations of known features are also utilized to constrain the final selection of models. The result is one or more superior models which, in the latter case, are not statistically distinguishable from each other with respect to the quality of fit. They represent the best description of the thorium surface distribution, based on the quality of the data and the limitations of the modeling process.

Data fields extending about 30° in longitude have been found optimum for these deconvolution studies, providing regions of significant size to generate an adequate model. The isotropy of the detector has the virtue of permitting observations to be made beyond the ground track, although with less certainty than if data had been obtained over these areas. It is possible to model up to 6° beyond the data track, depending on the size of the region and the relative concentrations involved.

Figure 4 shows a comparison between observed and deconvolved profiles along two strips of latitude for the Aristarchus region. As expected, the deconvolved profiles show sharper borders and greater contrast than the undeconvolved. As a validation check, the sum of the observed data within a given field has been compared with the sum of model values over the same field. The two values agree within 1-2%, demonstrating that the sum of the residuals is close to zero.

Mapping

Initial results from the Apollo gamma-ray spectrometer featured count rate maps of lunar radiation within the energy band from 0,55 to 2.75 MeV. Prior processing consisted of data selection, correction for variations in orbital altitude, and assignment by location with or without the removal of background contributions due to the cosmic gamma-ray flux and induced radiation from local material of the spacecraft. A color map using 5° squares for the Apollo 15 ground track was published in Metzger et al. (1972). Black and white maps using 5° squares for the Apollo 15 and 16 ground tracks were published in Arnold et al. (1973) and Metzger et al. (1973). The latter is shown in Fig. 5. A more detailed count rate color map using 2° squares for both ground tracks appeared as part of a set of lunar orbital data maps in the Proceedings of the 4th Lunar Scienc, Conference in 1973. For this map, the continuum and cosmic-ray induced radioactivity contribute-ons were also removed. The natural radioactivity ranged over more than a factor of 20 and was presented in seven intervals. Confidence in this map was fortified by the reproducibility of data from successive spacecraft orbits and by comparing regions overflown by both missions (Metzger et al. , 1973).

From these early maps (e.g. Fig. 5) it was clear that enhanced natural radioactivity is confined to broad highland and mare regions on the lunar nearside, and that limb and farside highland concentrations of Th, U and K are low, below values typical of terrestrial basalts. The single exception

within the two farside data tracks occurs near the crater Van de Graaff. Nearside maria show a striking contrast between east and west, with radioactivity in the west averaging about 2.5 times that seen in the east. This broad distribution of high radioactivity throughout the western maria points to a genetic relationship for that entire complex (Arnold et al., 1973), i.e., boundaries of individual.ly named units such as Mare Imbrium, Oceanus Procellarum, and Mare Nubium, do not necessarily correspond to compositional boundaries. Within the western maria, detailed structure is seen, in particular three localized regions containing the highest levels of lunar radioactivity seen to date. All three are associated with nonmare regions within the western maria (Metzger et al., 1973). From this, as well as the distribution of radioactivity in the western highlands bordering Mare Imbrium and Oceanus Procellarum, it has been suggested as an alternative to the lateral mixing of impact ejects, that this material in which most of the lunar radioactivity is carried, and which is known as KREEP (Taylor, 1982), was emplaced by the fractionation of magma from the interior over a broad area of the western nearside. This would have occurred prior to the impact excavation of Mare Imbrium and the subsequent covering of the Imbrium-Procellarum region by mare basalt flows (Metzger et al. , 1973). Several hundred kilometers beyond the western boundary of Oceanus Procellarum the concentration of natural radioactivity falls off rapidly through regions around the limb into the western farside highlands (90°-1800 W) where the concentrations are noticeably lower than those of the eastern farside highlands (90°-180° E), particularly over the northerly track of Apollo 16.

Early maps were also published for Fe and K in 1974 and 1976 respectively, both based on regional values derived from response function

and interpolation. Most of the processing and plotting work has been performed by the Astrogeology Branch of the U. S. Geological Survey (Eliason and Soderblom, 1977; Arnold et al, 1977).

Results of Response Function Analysis

Initial results from response function analysis described 28 lunar regions in terms of Fe, Mg, Ti, Th, and K concentrations with Apollo 15 data and four elements with Apollo 16 data, Ti being omitted from the latter due to a lack of consistency (Metzger et al., 1974). The analysis proceeded as described previously, except that the discrete spectrum was unfolded in two steps according to energy. Since the pulse height spectrum above 5 MeV is dominated by O, Fe, Ti, and Al, the data from 5-8 MeV was fitted with these four monoelemental response functions to obtain their individual contributions. Then the response of these four elements was subtracted and the resultant spectrum from 0.75-5 MeV analyzed for Th, K and Mg. Concentrations were obtained by applying unit concentration gamma-ray fluxes from Reedy et al. (1973).

The expected chemical contrast between mare and highland regions was seen nearly everywhere, with concentrations of the five elements determined found to be greater in the maria than in the highlands. The greater abundance of Fe and Th in the eastern farside regions than in the western was noted again, as was the extension of this asymmetry to the lunar limbs. The Van der Graaff region appeared to be unique, with Fe and Mg concentrations typical of highland regions, but Th and K concentrations typical of eastern maria.

analysis (Frontispiece, 1974 and 1976). The Fe map has four intervals of concentration ranging from less than 6.5% to more than 12%. Notable is a farside asymmetry with the Fe concentration being higher in the east than in the west. The K map, with some gaps in the ground track, is divided into five intervals of concentration ranging from less than 800 ppm to more than 2500 ppm.

Binning based on areas greater than 2° by 2° is necessary for elements with less sensitivity than Th, particularly where the concentration is low or the observing time is small. Larger areas are also often desired based on geological classification. Compositional results from the AGRS were initially reported for regions defined only as longitudinal bands within each ground track (Metzger et al., 1974), but such an approach often combined areas displaying clearly different surface characteristics such as albedo and typography. Therefore, more detailed outlines were developed that combined many adjacent 1° x 1° units of area into fairly homogeneous regions. Consideration was also given to including an adequate amount of data for analysis. Regional boundaries are mostly geographical, but some regions have been created to identify geochemical distinctions and for comparison with other data sets. These regions are defined in Metzger et al. (1977), with some minor revisions and two additions in Haines and Metzger (1980). They have been used in many of the papers discussing orbital geochemical results.

Later maps, several of which will. be discussed below, incorporate more carefully developed gamma-ray data bases and i nterference corrections, as well as more sophisticated processing techniques of normalizing, smoothing,

A second response function analysis carried out by Bielefeld et al. (1976) incorporated a number of significant improvements (Trombka et al., 1979), A revised and expanded library of gamma-ray line source strengths was used, based on additional nuclear data (Reedy, 1978). The data set was recompiled based on stricter selection criteria and more careful adjustments applied to corrections for variations in instrument gain, offset, live time, and spacecraft altitude. The pulse height spectrum was separated into eight background components in addition to the discrete line contribution. The lunar continuum was redefined by subtracting a total line spectrum component calculated from an average surface composition derived from ground truth. Separate continua were defined for Apollo 15 and 16; the 5% increase in the continuum of Apollo 16 reflected a mission-to-mission increase in the incident cosmic-ray flux.

After accumulating the data by region and subtracting the background, the matrix inversion analysis was performed on the entire discrete line component in one step rather than using two energy intervals as in the initial analysis. In addition to fixing the concentrations of O and Si as before, the value for Ca, which could not be usefully determined, was also fixed at a single representative value.

Four elements, Th, K, Fe, and Mg, were determined for sixty regions, among them the entire ground track, computed separately for Apollos 15 and 16. Interference from oxygen prevented useful results for Ti. In the earlier (1974) analysis, ground truth normalization of the elements from cosmic-ray-induced results were based on a comparison between Apollo 11 soil

sample data and the Mare Tranquillitatis regional values. In this analysis the normalization was more broadly based. Soil chemistry from several landing sites was associated with broad orbital regions, from which mean concentrations for the entire Apollo 15 and 16 ground tracks were calculated by folding in the fraction of the ground track covered by material of each type. Normalization factors for Fe and Mg were then calculated from the ratio of their modeled mean concentrations to the concentrations obtained by matrix inversion of the entire ground track.

Generalized estimates of error were made in terms of time independent and time dependent components. Validation checks produced positive results. Useful regions were limited to areas in which more than 2,000 seconds of data was available.

Regional results included the mean compositions of four eastern maria. Mare Serenitatis, Mare Fecunditatis, and Mare Tranquillitatis were found to be broadly similar, although K and Fe concentrations in Mare Serenitatis were about 20% greater than in Mare Fecunditatis and Mare Tranquillitatis. Mare Smythii, with lower concentrations of Th, K, Fe and Mg than the other three eastern maria, displayed a composition closer to that of highland regions. However, the Smythii basin includes a portion not covered by mare basalt flows. Intramare differences were noted for Mare Tranquillitatis and Mare Serenitatis (Reedy et al., 1975).

The three local regions of strikingly high natural radioactivity seen in the west, south of Archimedes crater, south of the Fra Mauro formation, and at Aristarchus, showed compositional distinctions despite similar Th

content. The actual location of these maxima was discussed, and it was concluded that the peak value is probably north of the ground track in the Archimedes region, might be north of the ground track at Fra Mauro (this based in part on data from the Apollo 14 landing site), and iscontained within the ground track at Aristarchus.

Across the central equatorial highlands from 30°E to 4°W, the KREEP component containing the bulk of the Th, U, and K radioactivity increased continuously, while Fe and Mg values remained typical of the highlands. The Van de Graaff region appeared less chemically distinct from its surrounding highlands than in the first response function analysis (Metzger et al., 1974), and it was judged that the chemistry is consistent with a mixture of mare and highland material or an intermediate mare chemistry similar to Mare Smythii. A farside asymmetry in Mg suggested by the 1974 analysis was not apparent in these results.

Energy Band Analysis

Thorium

As a basis for developing the regression line of known concentration vs net lunar counting rate, thorium concentrations for more than 50 regions, each derived separately by library function analysis and photopeak analysis, were compared (Metzger et al. , 1977). The fine correlation confirmed the quality of both sets of results. Regional concentrations for the resulting regression line were represented by weighted averages of the values from both techniques. The energy interval used was the wide 0.55-2.75 MeV band

discussed previously, Prior processing of the band data consisted of normalizing for variations in gain, zero drift, live time, spacecraft altitude, and local elevation, and the removal of nonlunar background components. The data was examined on an orbit-by-orbit basis and subjected to a set of criteria for acceptance. To apply both data sets to the same regression analysis, Apollo 16 data was normalized to Apollo 15 by comparing east and west crossover regions based on 5° x 5° unit areas. The significant difference in observed count rates was the result of higher cosmic-ray and interplanetary electron fluxes during the Apollo 16 mission.

Examination of the reference set of concentrations vs count rates showed a need for two fits, a straight line for ten regions covering the nearside central highlands and the general vicinity of Van de Graaff on the far side, and a nonlinear relationship for all the rest. After derivation, the fits were applied to generate Th concentrations with associated uncertainties for an expanded set of 144 regions (Metzger et al., 1977). The twelve components of uncertainty identified and quantized included the effect of non-thorium chemical variations, the effect of which was found to be small relative to the intensity of the wideband signal. Validation checks consisting of consistency between composite and subdivided regions, regional crossover comparisons between Apollo 15 and 16 data, and ground site soil composition comparisons were all favorable.

The data generated from this Th analysis, processed for color map presentation at the United States Geological Survey (USGS) Flagstaff Image Processing Facility, is shown in Fig. 6, Apollo 15 and Apollo 16 data tracks are superimposed on a rectangular grid providing coverage of ±50° in

latitude, ±180° in longitude, A schematic base map delineates the Mare Imbrium-Oceanus Procellarum complex, the eastern maria, major limb and farside basins, particularly along the ground tracks, and some local features. The input data, prepared by Robert Radocinski at JPL in the form of corrected count rates on a 1° x 1° grid, have been smoothed to a continuous distribution using weighted-average spatial filters ranging in picture element dimension from 3x3 to 39x39, with less weight given to the larger sized filters and data points of larger uncertainty (Eliason and Soderblom, 1977). The effective spatial resolution of the final image is about 2° of surface area. Concentrations are derived from the regression relationship of Metzger et al. (1977). Seven color levels have been used over the concentration range; the key is given with the figure.

Figure 6 shows vividly the degree to which radioactivity is concentrated in the western nearside surface of the Moon. With the color scale used, the two northern features of highest concentration appear to be about 8° wide in longitude prior to the application of spatial deconvolution; the southern feature is somewhat broader. Note that the Aristarchus Plateau and Crater (48°W, 23°N) and the Archimedes Crater (4°W, 20°N) are shown on the base map. Continuation of the zone of notably radioactive material beyond the boundaries of the western maria, especially into the central equatorial highlands, is more striking than observed before (Arnold et al., 1977). In contrast, color transitions occurring within 3° or less of mare-highland borders can be seen in a number of places in the east. On the farside, the region of Van de Graaff enhancement includes that feature at 172°E, 26°S and extends more than 10° to the east.

From the color map it can be seen that the general distribution of surface radioactivity on the Moon is, in order of decreasing concentration, the western maria, eastern maria, nearside highlands, limb and farside highlands. Although based on only 23% of the Moon, photogeologic associations suggest that this result will hold for the entire surface. The average Th concentrations for major regional groupings and their associated uncertainties are given in Table 1.

In the western maria, excluding the nonmare enhanced areas of Aristarchus and Fra Mauro (17°W, 8°S), regional Th concentrations range from 3-6 ppm, with an average value of 4.6 ± 0.4 ppm. Thorium shows a pronounced decrease in concentration going from east to west over both ground tracks in Oceanus Procellarum (~30°-85°W, 12°S-30°N), particularly as the mare-highland border is approached. In the east, Mare Serenitatis (~10°-30°E, 16°-28°N), Mare Tranquillitatis (~20°-45°E, 5°-16°N), and Mare Fecunditatis (42°-60°E, 8°S-5°N), all average about 2.0 ppm Th, without a significant difference. Within these maria and away from highland borders, concentrations are indistinguishable from or somewhat higher than total mare values, the latter ascribed to a degree of observational mixing from highland areas within the field of view. Additional contrast is seen within Mare Serenitatis and Mare Tranquillitatis, concentrations in the east being lower than in the west. Lower Th values are observed for Mare Crisium (~50°-65°E, 10°-20°N) and Mare Smythii (~80°-92°E, 7°S-6°N) which lie closer to the eastern limb. Mare Undarum (~60°-72°E, 0-10°N), a small mare between Crisium and Smythii, shows no enhancement relative to its surrounding highlands.

Average Th concentrations for the seven large highland areas listed in Table 1 show a range amounting to a factor of six. Several local regions of higher radioactivity, such as Fra Mauro, the Apennine Bench, the Haemus Mountains and Van de Graaff have not been included. Differences in concentration with location must reflect the distribution within the central and nearside highlands of a greater proportion of those highland basalt rock types which carry the radioactive signature. Substantially lower Th values are found in the west limb than in the east limb, The west limb average of 0.38 ppm is also lower than the average in the farside highlands whether west or east, making the western limb the area of lowest radioactivity thus far observed on the Moon. The lowest Th value among the 144 delineated regions is a 10° x 12° area located just beyond the western limb and centered a few degrees north of the equator, for which the measured Th concentration is 0.24 ± .10 ppm. The western hemisphere therefore possesses the highest and lowest levels of radioactivity mapped to date. By contrast, the east limb regions are relatively invariant with Th concentrations of 0.62-0.82 ppm. The difference in radioactivity between east and west limb regions is striking, amounting to a factor of two. This is about half the ratio between the nearside central highlands and farside highlands. Comparison of the western and eastern farside highlands confirms the asymmetry noted previously (Metzger et al. , 1973; 1974) as a 50% greater Th concentration in the east.

The nearside western highlands show considerable variation. This appears to be the result of their proximity to the large KREEP-rich area which surrounds and underlies Mare Imbrium and Oceanus Procellarum. Once again the east shows less contrast, Th ranging from about 1.1-1.4 ppm

between 55° and 90° east longitude. The highland regions situated between the eastern maria from 40°E to 62°E are some 20% higher in Th than the highlands between 55°E and 90°E, and are roughly equal to the levels measured in Mare Crisium and Mare Smythii. It follows that the contrast in Th content between Mare Crisium and Mare Smythii on the one hand, and these intermare highlands on the other, is less than that versus the maria lying to the west.

Moving eastward across the central highlands on the Apollo 16 ground track, the Th concentration drops sharply and steadily from values close to 8 ppm at the western edge near Alphonsus (3°W, 13°S) to 2 ppm at Descartes, twenty degrees to the east, then remains essentially constant eastward across the remainder of the central, highlands. Not only does the 2.2 ppm average exceed by a large amount that found elsewhere in large highland areas, it is also greater than the average value of 1.82 ppm in the eastern maria.

By dividing the lunar surface into chemical provinces and assigning Th concentrations to them by analogy to measured areas, estimates of the Th content of the Moon's entire surface have been made (Metzger et al. , 1977). For a model consisting of five provinces with the associated Th
T2 concentrations listed in Table 2, the whole moon average concentration is 1.29 ppm. This type of calculation has also been used to estimate crustal abundance.

Titanium

The second element for which a set of regional concentrations was derived by energy band analysis was titanium (Metzger and Parker, 1979). Compared to other elements such as Fe, Si and O, which also produce characteristic gamma rays by means of cosmic-ray induced activation, deriving Ti concentrations from the Apollo data is more difficult because its abundance is relatively low, its strongest lines occur at high energies where the detector response is relatively poor (only partly offset by a lower underlying background), and because other elements, particularly Fe and O, contribute significant levels of interference over the same energy interval. The impetus for the effort to obtain Ti results lies in its importance in characterizing rock types, particularly for distinguishing various mare basalt compositions and the conditions under which they were formed (Rhodes et al., 1975; Papike and Vaniman, 1978). Of the elements accessible by orbital gamma-ray spectroscopy, Ti and Fe are the two most useful to distinguish mare basalt rock types in order to determine their relative abundance and distribution (Davis, 1980; Metzger and Drake, 1990).

The energy interval chosen for extracting Ti concentrations from the AGRS data was 5.95-6.37 MeV, a choice dictated principally to minimize contributions from several Fe lines. Generating the regression curve requires a set of regions whose concentrations are known. The Th regression curve was obtained using a set of regions whose concentrate ons were determined by combining results from response function analysis and photopeak analysis. Unfortunately, the Ti lines are too poorly resolved in a scintillation detector for photopeak analysis, while an attempt to

construct a regression curve from a set of Apollo 15 concentrations derived by response function analysis proved unsatisfactory. The regression curve was therefore generated in a different manner, namely by utilizing Ti concentrations of returned soil samples at the various landing sites. These were plotted versus the energy band count rate of representative lunar regions, i.e., from regions within which the site was located, or regions were close by and believed to be geochemically equivalent to the site. When the interference due to Fe, Ca, Al, O, and Si was removed, a good correlation was obtained. Iron was removed on a region-by-region basis, in proportion to the count rate ascribed to Fe from an analysis of the 6.37-8.00 MeV band in which it is the major variant; the other four elements were treated as a group in the manner employed for bulk element interference in the Th analysis. The Ti regression curve is shown in Fig. 7. The uncertainties of the points are the root-mean-square values of the random error components for the observed count rates with unit weighting applied to the concentrations. Note that the Apollo 17 landing site at Taurus-Littrow (28°E, 20°N) provided soil samples derived from the local mare as well as the highlands, the first taken to represent the region containing the site, the second paired with the adjacent highlands region to establish an additional point for the regression set.

Concentrations were produced for 137 regions. Values range from no detectable Ti to a level of 4.4% over a portion of Mare Tranquillitatis. Figure 8 shows the USGS color map prepared from this data set.

Areas of titanium enhancement over the eastern nearside are clearly associated with mare regions. Mare Crisium is the notable exception among

the five eastern maria surveyed. Though limited by a short observing time, the measured value of 0.9% is comparable to the 0.7% value found for the soil returned from the Luna 24 site which is located in Mare Crisium (Blanchard et al., 1978). No local concentration significantly greater than the Apollo 11 soil sample value of 4,5% was seen within the ground track. Among the eastern maria, Mare Tranquillitatis contains the highest concentration of Ti at 3.1%, followed by Mare Serenitatis with 2.4% Ti and the northern half of Mare Fecunditatis with 1.9% Ti. Variations in concentration can be seen within all three of these maria and appear particularly pronounced in Mare Fecunditatis. Mare Smythii is only partially covered by mare basalts; the north-south division seen in Fig. 8 corresponds to the debarkation between the flooded and unflooded portions of this basin. A corresponding separation into two regions showed that the flooded portion with 1.4% Ti was 70% higher than the unflooded portion, consistent with expectation, although measurement precision is limited by the short observing time. The higher Ti concentrations extend several degrees beyond the eastern border of Mare Smythii. Without the lower Ti contributions from Mare Smythii and Mare Crisium so that the eastern maria are represented by the three larger and more westerly units (Tranquillitatis, Serenitatis, and Fecunditatis), the measured average value rises from 2.1% to 2.4%. Titanium concentrations for major regional groupings are shown in the third column of Table 1.

Comparable Ti levels are found in the western maria, but vary with location. High concentrations are seen south and west of the Aristarchus Plateau (Fig, 8). The latter has the highest regional Ti concentration measured in the western maria (4.1%), The average for the area surveyed

within Oceanus Procellarum and Mare Imbrium is 2.0 ± 0.4%. A significant difference appears to exist between the eastern and western portions of Mare Imbrium (9-35°W, 20-30°N), the Ti content in the western portion being about 50% greater. Along the northern track of Oceanus Procellarum, regional values range from 1.5% to 4.1%. Along the southern track, the Ti content increases west of Mare Cognitum (24°W, 10°S) but shows a lower average concentration than found in the north. Regions on both sides of the mare-highland western boundary appear to have Ti concentrations intermediate between those of Oceanus Procellarum and the west limb highlands.

In the highlands, Ti concentrations are everywhere distinctively lower than in maria and dark mantled highland areas except in the southern highlands bordering Oceanus Procellarum, the Haemus Mountains (10°E, 18°N), an eastern limb region twenty degrees south of Mare Smythii, and the eastern portion of the Mendeleev basin (lLO"E, 5°N). The apparent enhancement at 110°W, 10°S is a spurious edge effect. The nearside-farside contrast between high and low Ti values mirrors the confinement of maria regions largely to the nearside. The lowest abundances on the nearside are found in the western portion of the central highlands and north of the Orientale basin. Along the southern track five changes in trend can be seen between 40° E and 20° 'W, each time conforming to the predominance of mare or highland material in the field of view.

The entire highlands viewed averages 0.8 ± 0.3%, somewhat higher than expected from measurements on returned samples. Major highland regional averages compiled in Table 1 are quite uniform, apart from the lower value observed in the western limb highlands. On the farside, Fig. 8 shows that

higher values are more common in the north than the south. The average difference in Ti concentration between the limb-farside data tracks amounts to more than 50%. Comparisons of the crossover regions, the highland east and nearside regions, and western limb regions, show that this is not a systematic difference between Apollo 15 and 16. Another farside asymmetry is visible in the south where concentrations below 0.2% are more dominant in the west than *in* the east. The sharp contrast in Ti abundance between the Apennines (0°, 20°N) and the Haemus mountains suggests a demarcation of geologic provinces. The highest farside concentrations occur within the eastern two-thirds of the Mendeleev basin. This enhancement is quite pronounced and trends lower both east and *west* of the basin, The value for Van de Graaff and the area to the east of it is unusually low in Ti, confirming an earlier result (Metzger et al. , 1974).

A second energy band analysis for Ti (Davis, 1980) employed the 4.78-6.99 MeV band which, because the energy interval is wider and extends to lower energies than the 5.95-6.37 MeV band, offers better statistics but requires a much larger correction for iron interference. Mare Fecunditatis was found to have high concentrations of Ti less uniformly distributed than those in Mare Tranquillitatis. These high concentrations extend to the Taurus-Littrow area. For the same set of regions the range of Ti concentrations is 20% greater than that found in the earlier analysis. Some significant differences in regional concentrations exist between the sets but this analysis also finds high Ti levels along the northern farside track.

Iron

Initial observations on the concentration of iron were based on a count rate map from 2.75 to 8.60 MeV, a portion of the energy spectrum which is free of interference from natural radioactivity (Frontispiece, 1977). Following this, a narrower energy band more specific to Fe, from 6.37 to 8.00 MeV, was tried. Because of excessive interference due to Ti in this range, a third interval was chosen, this time 6.99-8.89 MeV (Davis, 1980). A regression *curve* was generated in a manner similar to that used for Ti, being based on Fe values in soil samples from eight landing sites, Instead of applying unit weighting to site concentrations, this analysis was refined by using the method of York (1969) to incorporate uncertainties associated with the ground site concentrations as well as orbiting count rates in deriving the slope and intercept. The certified AGRS data set was applied to the regression curve to produce 137 regional values of concentration (Davis, 1980), as well as a USGS color map of the entire ground track which is shown in Fig. 9.

F9

Iron concentrations are seen from the map to be consistently higher in mare regions than in the highlands. Within the extended western maria, concentrations of Fe are highest in Mare Imbrium and northwest Oceanus Procellarum but remain high throughout Oceanus Procellarum except in the regions around Aristarchus and Fra Mauro. Davis (1980) has pointed out that concentrations in the eastern maria appear to possess somewhat more variability than those in the west. Otherwise, east and west maria values are fairly comparable and more than double the mean concentrations in the highlands as a whole. Mare Serenitatis and Mare Crisium contain the highest

concentrations observed, the former in agreement with response function analysis (Bielefeld et al., 1976), while Mare Smythii contains the lowest. For Mare Crisium, the map understates the abundance of 14.4% tabulated by Davis. Occurrence of a greater concentration of Fe in the mare basalt-covered portion of the Smythii basin than in the unflooded portion is clear from their individual regional values and is visible on the map. Tabulated concentrations in the highlands range from 3% to 9%, with the lowest values found, as for Th, in the western farside highlands and western limb.

The highest Fe highland concentrations are found in the eastern nearside highlands. Area-weighted mean concentrations of Fe for major regional divisions based on the values found by Davis (1980) are given in the last column of Table 1. Concentrations in the farside highlands are well below those of the nearside highlands with the exception of the central highlands. The east-west asymmetry displayed by Th in the limb regions is also found for Fe but the farside difference is insignificant.

Concurrent with this analysis, Haines and Metzger (1980) produced a set of Fe concentrations for 37 highland regions in order to study highland crustal models. These utilized the same data set and the same energy interval, but a different regression curve, one based on ten ground site values. In addition, the flux at each lunar region was corrected for the influence of neighboring regions based on *a priori* knowledge of mare-highland borders.

A comparison of this set of regional concentrations with those of Davis shows close agreement with Apollo 16 regions and somewhat lower values for

those of Apollo 15. This reflects both the difference in the two regression curves, and a difference in the Apollo 16 to Apollo 15 normalization factor as derived from the ratio of responses within eastern and western regions of trajectory overlap. The Haines-Metzger set does not show the north-south farside highland asymmetry suggested by Davis.

Regions high in Th are also relatively high in concentrations of rare earth elements. Some of the latter (e.g. Sm and Gd) have very large thermal neutron capture cross sections, the effect of which is to reduce the flux of thermal neutrons and thereby lower the apparent concentrations of elements emitting gamma rays following neutron capture. Indications of this flux depression effect were found in the results of response function analysis for Fe, by comparing its strong neutron capture lines near 7.6 MeV which should show the depression effect, with its inelastic scatter line at 0.847 MeV which will not be affected (Metzger et al., 1974; Trombka et al., 1977). On the other hand, a map of the integral count rate in an energy band representing the inelastic scatter line of Fe (Arnold et al., 1978) failed to show any contrast between the two types of Fe reactions. To resolve this question, Davis and Bielefeld (1981) performed an energy band analysis over the 0.803-0.872 MeV interval to produce a set of Fe concentrations based on the inelastic scattering reaction line. The count rate was corrected for interference due to varying concentrations of Th, U, and K, and an empirical test was used to demonstrate insensitivity with respect to an expected contribution from an Al line at 0.844 MeV. Davis and Bielefeld found a satisfactory correlation between their inelastic scattering concentration set and the prior Fe set of concentrations based on neutron capture (Davis, 1980), and therefore no consistent evidence for thermal neutron flux depression in the Fe neutron capture data.

Potassium

A narrow energy interval, from 1.44-1.51 MeV, served for the energy band analysis of potassium (Parker et al., 1981). This band was chosen to be asymmetric around the single 1.46 MeV gamma-ray line emitted by radioactive K-40 in order to limit interference from a strong gamma-ray line at 1.37 MeV. Regional corrections were applied to remove the interference due to Th + U. Because production rates for naturally radioactive K, like Th, are relatively well known, the reference concentrations of K used to establish the regression curve were also regional values obtained by the response function analysis of continuum-subtracted net energy spectra (Bielefeld, et al., 1976). Separate fits were developed for the Apollo 15 and Apollo 16 data sets.

The concentrations obtained from the regression curves are in reasonable agreement with corresponding ground site soil values. These results are lower on average than those from the earlier response function analysis (Bielefeld et al., 1976). They range from 100-600 ppm in t:he farside highlands, 300-700 ppm in the limb highlands, and nearside highlands from 700 ppm to well over 2,000 ppm. High values are seen over the central highlands, particularly in the west. Eastern maria values range from 400 ppm in Mare Crisium to 1,400 ppm in the western portion of Mare Tranquillitatis. Aristarchus, Archimedes, Fra Mauro, and Mare Cognitum, the regions containing the highest observed values of Th, are correspondingly high in K, the Fra Mauro value being 2,700 ppm. Certain other regions such as Ptolemaeus crater arid the Apennine Bench Formation also show high concentrations .

Earlier results for K were confirmed, The average value of K/Th is lower than that of the terrestrial crust (Metzger et al., 1973), reflecting the depletion of volatile elements from the Moon (Taylor, 1986), and is inversely proportional to Th concentration (Schonfeld, 1977; Metzger et al., 1977) . Figure 10 plots energy band analysis-derived regional values of Th Vs . response function analysis concentrations of K, the latter taken from Bielefeld et al. (1976), but reduced by 140 ppm to improve the agreement with lunar sample data, based on a comparison by Schonfeld (1977). The major chemical provinces are distinguished by symbol. Included for comparison are average ratios for rock and soil samples from the various landing sites. The K/Th ratio decreases asymptotically with increasing Th concentration over the entire range and for all provinces. Values of K/Th extend from 260 to 1,900, primarily reflecting the relative proportions of anorthosite, basalt, and KREEP components present within a given region. 'l'he corresponding range of K/U, based on a Th/U ratio of 3.8, is about 1,000-7,200.

F10

The farside and limb highlands show the largest range in K/Th ratio, partly because the low concentrations in these regions increases the scatter of the data, but also reflecting real differences in concentrations and therefore in proportions of the three principal highland rock components, the anorthosites, which are predominantly plagioclase feldspar, the norites, a set of Mg-rich plutonic rocks, and KREEP (James, 1980; Taylor, 1982). The three west limb and three east limb data points fall into two widely separated groups due to their approximately equal K content coupled to sharply different Th levels. The farside and limb highland values cover a

range about three times greater than all the other provinces combined. Note that the average K/Th ratios for the nearside highlands, eastern mare, central highlands, and western mare, each represented by at least five regions of orbital data, decrease in the same order as the soil sample average ratio from their corresponding sites. The nearside highlands points comprise a tight set, considering that the group is composed of two regions in the west and four regions in the east. The cohesiveness suggests that their compositions may be fairly uniform on average. Seven non-maria regions within the western maria are plotted separately and conform to the general trend.

Calculating the average highland abundance of K from the mean orbital Th concentration plus sample-averaged ratios of Th/U and K/U yields 600 ppm (Taylor, 1982, p. 231), in excellent agreement with the value from energy band analysis of 580 ppm (Parker et al., 1981).

Spatial Deconvolution

Aristarchus and its surroundings was the first area to which the spatial deconvolution technique was applied (Haines et al. , 1978). It was subsequently reworked after a misalignment of the data field was discovered (Etchegaray-Ramirez et al., 1983). Besides Aristarchus, *regions* centered on Mare Imbrium, the Apennine Mountains, Mare Smythii and the central highlands have also been deconvolved. Each data field has been modeled into about a dozen constructs of varying size and shape. The end product has been not one model, but a family of best fits which are not distinguishable statistically, and which show no major variation in model shape, Figure 11

shows a composite of representative superior models of the Aristarchus, Imbrium, and Apennine data fields comprising a swath about 70° in longitude and 20° in latitude. Associated concentrations are best fit mean values. Although the improvement in spatial resolution and accuracy is accompanied by a 50-100% loss in precision, the concentration range and uncertainty for a given construct within the family of best fits both decrease with increasing observing time and construct size.

Included in the area displayed in Fig. 11 are two of the three most radioactive regions within the Apollo 15 and 16 ground tracks. In both cases, the restoration of lost contrast has more than doubled the estimated peak Th concentration at the sites. The corresponding improvement in spatial resolution has made it possible to localize the western hot spot from the entire Aristarchus region (Bielefeld et al., 1976) unambiguously to the crater and its ejects blanket. Similarly to the east, the source of the enhanced Th concentration, previously referred to as south of Archimedes (Metzger et al., 1973), is found to be the crater itself and its immediate surroundings. The latter result is the more striking because no gamma-ray data was acquired over Archimedes crater, which is centered 3° north of the Apollo 15 ground track. The association has been made by the ability to deconvolve beyond the ground track.

The deconvolved area shown in Fig. 11 contains a wide range of Th concentrations, from 1-20 ppm. For constructs modeled in more than one data field, the most reliable result based on construct location and the number of superior models has been used. The concentrations are generally consistent from field to field. More compositional diversity is seen in the

Archimedes and Apennine regions than in the Imbrium region, consistent with photogeologic interpretation. High Th concentrations are not confined to ejects-rich regions such as Aristarchus, Timocharis, and possibly Lambert, but are also found in mare regions as well. Some regions of Th enhancement are clearly associated with surface features while others are not. The abundance of Th on the Aristarchus Plateau is not uniform, higher concentrations being seen north of the crater, possibly due to a greater contribution of ejects. Combining Archimedes with the Apennine Bench provides a larger construct with a Th concentration of 12.9-13.0 ppm, but a fit which is poorer than with separate regions. In eastern Mare Imbrium the Th range of 3.4-4.6 ppm is decidedly below the 5.6 ± 0.4 ppm undeconvolved measurement (Metzger et al., 1977). This change is the result of the identification and separation of the enhanced Timocharis region. Without the latter, the deconvolved value *rises* to 5 ppm. These results imply that concentrations of other elements are also likely to vary substantially within this and similar regions.

In the Th energy band analysis, the flooded portion of the Smythii basin was found to have a Th concentration only 5% greater than the entire basin. When spatial deconvolution was applied to a region which included Mare Smythii (Haines et al., 1978), the distinction became clear, with 1 .7 ppm and 1.2 ppm for the flooded and unflooded portions respectively. The former value is more comparable to the 2.1 ppm average concentration observed for other eastern mare than the undeconvolved value of 1.4 ppm for all of Smythii. As mentioned above, this mare - highland dichotomy within the Smythii basin has also been seen for Ti and Fe. The most significant result from the improved spatial resolution in this area has been the

discovery of local highland regions with Th concentrations of 2.5 - 3.5 ppm, comparable to or slightly greater than those of mare basalts. The probable cause is the occurrence of highland volcanism at a time approaching or just following the termination of intense surface bombardment (Haines et al. , 1978) .

APPLICATIONS OF THE DATA

The energy band and response function methods have succeeded in extracting sets of Th, Fe, Ti, K and Mg surface concentrations and associated uncertainties from two sets of gamma-ray orbital measurements. This section offers a brief summary of various lunar issues which have been addressed with information from the AGRS experiment. Besides the specific references cited, Taylor (1975, 1982), Hartmann et al.. (1986), and Phillips (1986) offer comprehensive overviews of lunar science.

Geochemical Comparisons

Comparisons with landing site sample compositions serve to validate the orbital data as well as to extend its usefulness . Table 3 presents average soil concentrations of Th at nine Apollo and Luna sites, together with the concentration of the contained or closest 2° x 2° or 5° x 5° orbital region.

The lower sample values for Luna 16 and 24 soils may be due to local variation. The Luna 16 site is located well into Mare Fecunditatis and the orbital value of Th is typical of eastern maria (Table 1). The Apollo 14 site is 170 km from the orbital sample and the difference in this region of high contrast can be accounted for by a gradient between the *two* locations. The consistency between orbital measurements and site soil averages demonstrates that gamma-ray orbital data can indicate the degree to which local surface concentrations are typical of the area analyzed from orbit, which in turn provides confidence in the results elsewhere on the Moon.

Magnesium has been measured from orbit by both the X-ray spectrometer and the gamma-ray spectrometer. A comparison of 22 regional Mg concentrations derived from the two experiments shows a correspondence within the uncertainty of the measurements (Bielefeld, 1977). An inverse relationship between Fe and Al concentrations which exists for Apollo soils and rocks (Janghorbani et al. , 1973) has been found to hold for orbital data as well (Bielefeld, 1977). Ultraviolet, visible, and infrared reflectance spectra of mare regions contain features which are associated with the presence of Ti and from which abundances have been estimated (Johnson et al., 1977; Piete'rs et al., 1980). Recent telescopic spectral reflectance observations have produced a nearside TiO_2 abundance map for the lunar maria (Johnson et al., preprint) showing good agreement with comparable Apollo gamma-ray values in collocating the highest concentrations seen within the Apollo data tracks.

Interelement correlations make it possible to extend the orbital observations to elements other than those measured directly. By applying

interelement correlations to the orbital data, Taylor (1.975, 1982) has constructed an extensive table of element concentrations for the estimated bulk highland composition, using direct measurements where they exist and sample-derived correlations where they do not.

Evidence of Volcanism

Spatial deconvolution of the region around Mare Smythii (Haines et al., 1978) has disclosed several areas to the southwest near the Balmer basin (70°E, 20°S) with Th concentrations greater than any undeconvolved values seen in the eastern highlands. This has been attributed to highland volcanism. A sharp chemical boundary seen between the Crisium and Smythii basins in the X-ray orbital measurements of Mg and Al, corresponding to similar contrasts in Th and Ti, is also indicative of separate episodes of volcanism (Andre, 1981).

In general terms, the presence of KREEP basalts in the lunar highlands has been proposed to be the result of ancient, pre-mare volcanism (Ryder and Taylor, 1976). Overall the Th distribution measured from orbit provides convincing evidence that the upper portion of the lunar crust throughout much and perhaps all of the Imbrium-Procellarum complex is dominated by KREEP basalts. Near the Apollo 15 landing site, several. studies have utilized the orbital gamma-ray and X-ray data, together with sample data and photogeologic studies dealing with morphology and age, to conclude that the Apennine Bench Formation (0°, 22°N) was the site of extensive KREEP volcanism, representing possibly the largest example of pre-mare KREEP volcanism on the lunar surface (e.g. Spudis, 1978).

Identification of Rock Types

From the returned sample collection, the occurrence 'of enhanced Th concentrations is interpreted as equivalent to the presence of KREEP basalt so that the Th distribution above 2 ppm becomes essentially a map of that rock type (Schonfeld and Meyer, 1973). With Th concentrations in the western limb and farside regions ranging from 0.3-0.5 ppm (Table 1), close to the level of uncontaminated anorthositic rocks, large highland areas must contain little or no KREEP basalt (Schonfeld, 1974).

Classifying mare basalts into three compositional groups based on Ti content, the Apollo results show that low Ti basalts are more abundant than either high Ti-basalts or very low Ti basalts (Metzger and Parker, 1979). The limited surface distribution of young high-Ti basalts indicated by the gamma-ray results argues for heterogeneous source regions rather than models that require either a homogeneous distribution of composition or continuously decreasing Ti concentrations with time (Head, 1976).

The mixing model technique has seen frequent use in lunar studies as a means of determining the proportions of comingled rock types. It is assumed that the chemical. composition of a site soil or breccia, or an area viewed from orbit is the result of adding linearly the contribution of each of the rock types present according to their abundance (e.g. Schonfeld and Meyer, 1972). Results depend on the choice of end-member components and the uncertainty in the elements available for the analysis. Most of the regions represented by AGRS data have been modeled with three and four component

end-member sets and compared with a similar analysis of highland soil samples (Haskin and Korotev, 1981). Mixing model studies of particular areas have utilized other data sets in addition to the orbital gamma-ray results; locations include Fra Mauro and the Imbrium basin (Hawke and Head, 1978), the Apennine Bench Formation (Spudis, 1978), the central highlands (Spudis and Hawke, 1981.), the Orientale basin (Spudis et al., 1984), and various other highland areas (e.g. Lucey and Hawke, 1988).

A different approach to the presentation of orbital geochemical data has been developed in the form of element concentration ratio plots in order to define petrologic units and to determine their geologic relationships (Davis and Spudis, 1985, 1987). The plots are divided into petrological classifications corresponding either to clustering of the orbital data, coincidence with sample compositions, or both.

Crustal Thickness

Comparison of elevation data (Kaula et al., 1972) with coincident concentrations of natural radioactivity have revealed a strong inverse correlation between elevation and natural radioactivity over both ground tracks, except in the central highlands and over mare regions (Trombka et al., 1973). Regions of high elevation are characterized by low natural radioactivity and vice versa.

Variations in elevation have been linked to changes in crustal thickness (Kaula et al., 1974). Generation of a crustal thickness map from gravity and elevation data (Bills and Ferrari, 1976) has permitted a comparison between surface Th and crustal thickness, revealing the striking F12 inverse relationship shown in Fig. 12 (Metzger et al., 1977). Correlations with crustal thickness have also been observed for Fe and Al (Schonfeld, 1977). These concentration-elevation-crustal thickness relationships clearly demonstrate that the highland surface is 'representative of the underlying crust, and that its initial character has not been destroyed by the lateral and vertical mixing due to bombardment (Metzger et al., 1977; Schonfeld, 1977).

Haines and Metzger (1980) have calculated values for the thickness and density of the lunar crust by means of orbital gamma-ray, lunar sample, and F13 seismic data. Figure 13 shows the regional values of density and crustal thickness plotted versus elevation. The results provide an insight into the mechanism governing the isostatic compensation of the lunar highlands.

Bulk Uranium Estimates

Heat flow measurements were made at the Apollo 15 and 17 landing sites, To extrapolate these local results to the entire Moon, orbital thorium concentrations and crustal thicknesses derived from elevation were combined in proportion to regional areas to calculate a global heat flow value (Langseth et al., 1976). From the global heat flow of 18 erg s^{-1} cm-z and assumed crustal values of Th/U, K/U, and Th content, a bulk U abundance of 46 ppb was derived.

Bulk U content can also be estimated based on surface concentrations alone. In the absence of a direct measurement of U, values can be obtained from the average concentrations of K and Th taken from the orbital data, together with returned sample K/U and Th/U ratios. Assuming that all the U is concentrated in the crust and the mantle is entirely depleted, then the crustal concentration combined with crustal thickness yields the bulk lunar U concentration. For a mean crustal thickness of 75 km, such a calculation has yielded a bulk U estimate of 30 ppb (Drake, 1986), The better established value for the Earth is about 20 ppb; whether the Earth and Moon have the same or different total concentrations of elements such as U is important in understanding the origin of the Moon.

CONCLUDING REMARKS

If the Ranger and Luna gamma-ray experiments are regarded as the infant efforts of a new technique, and the Venera surface radioactivity measurements as a major youthful activity, then remote gamma-ray spectroscopy came of age on Apollo. The availability of ground site comparisons have had a value beyond specific correlations by also validating the technique for this and future applications. Future experiments will bring further maturation as instrument capabilities improve and mission times are extended.

Since the Apollo experiment, scintillation detectors have been used in gamma-ray spectrometers on successive U.S.S.R. missions to Mars in 1974 and

1989 (Surkov et al. , 1980; d'Uston et al. , 1989). Application of the next generation of gamma-ray detector, based on high resolution germanium, in a spectrometer for the Mars Observer mission is at hand (Boynton et al, , this book) , A similar instrument is expected to be employed on a future Lunar Geochemical Orbiter mission (Phillips, 1986) , which with greater sensitivity, surface coverage, and duration, will provide substantially superior results to those from Apollo (Metzger and Drake, 1990). Until that time, the Apollo gamma-ray data set will continue to be one of the most valuable sources of present knowledge of the Moon.

Acknowledgements

The valuable reviews provided by Philip A. Davis, B. Ray Hawke, Robert C. Reedy and Ernesto Schonfeld have benefited the manuscript and reassured the author. My appreciation also goes to Davis for the interest and patience displayed in responding to requests for additional trial maps in his preparation of Figures 6, 8 and 9. Reedy and Larry Evans offered helpful suggestions in the tours-e of discussions on balancing the content of this chapter with theirs. Finally, a word of thanks to Peter Englert for his encouragement and refusal to allow me to miss the submittal deadline. The preparation of this chapter was carried out at the California Institute of Technology's Jet Propulsion Laboratory, under contract with the National Aeronautics and Space Administration.

REFERENCES

Andre C. G. (1981) Chemical rings of lunar basins from orbital x-ray data. Proc. Lunar Planet. Sci. 12A, pp. 125-132.

Arnold J. R. (1958) The gamma spectrum of the Moon's Surface. Proceedings of the Lunar and Planetary Exploration Colloquium, 1, #3, pp. 28-31, Space and Information Systems Division, North American Aviation Inc. , Downey, Ca.

Arnold J. R., Trombka J. I., Peterson L. E., Reedy R. C., and Metzger A. E. (1973) Lunar orbital gamma ray measurements from Apollo 15 and Apollo 16. In Space Research XIII, pp. 927-933, Akademie-Verlag, Berlin.

Arnold J. R., Metzger A. E., and Reedy R. C. (1977) Computer-generated maps of lunar composition from gamma-ray data. Proc. Lunar Sci Conf 8th, pp. 945-948

Arnold J. R., Da'vis P. A , and Reedy R. C, (19"?8) Gamma-ray maps of lunar titanium and iron (abstract) . In Lunar and Planetary Science IX, pp. 25-26. Lunar and Planetary Institute, Houston.

Barsukov V, L., Tarasov L. S., Dmitriev L. V., Kolesov G, M., Shevaleevsky I. D., and Garanin A. V. (1977) The geochemical and petrochemical features of regolith and rocks from Mare Crisium (preliminary data). Proc. Lunar Sci. Conf. 8th, pp. 3319-3332.

Berger M. J. and Seltzer S. M. (1972) Response functions for sodium iodide scintillation detectors. Nucl. Inst. Methods, 104, 317-333.

Bielefeld M. J., (1977) Lunar surface chemistry of regions common to the orbital X-ray and gamma-ray experiments. Proc. Lunar Sci. Conf. 8th, pp. 1131-1147.

Bielefeld M. J., Reedy R. C., Metzger A. E., Trombka J. I., and Arnold J. R. (1976) Surface chemistry of selected lunar regions. Proc. Lunar Sci. Conf. 7th, pp. 2661-2676.

Bills B. G. and Ferrari A. J. (1976) Proc. Lunar Sci. Conf. 6th, Frontispiece, Plate 3.

Blanchard D. P., Brannon J. C., Aaboe E., and Budahn J. R. (1978) Major and trace element chemistry of Luna 24 samples from Mare Crisium. In Mare Crisium: The View from Luna 24 (R. B. Merrill and J. J. Papike, eds.), pp. 613-630. Pergamon Press, New York.

Davis P. A., Jr. (1980) Iron and titanium distributions on the Moon from orbital gamma ray spectrometry with implications for crusts.]. evolutionary models. J. Geophys. Res., 85, 3209-3224.

Davis P. A., Jr. and Bielefeld M. J. (1981) Inelastic neutron scatter iron concentrations of the Moon from orbital gamma ray data. J. Geophys. Res., 86, 11919-11926.

Davis P. A. and Spudis P. D. (1985) petrologic province maps of the lunar highlands derived from orbital geochemical data. Proc. Lunar Planet. Sci. Conf. 16th, in J. Geophys. Res., 90, D61-D74.

Davis P. A. and Spudis P D. (1987) Global petrologic variations on the Moon: A ternary-di.agram approach, Proc. Lunar Planet. Sci, Conf. 17th, in J. Geophys. Res., 92, E387- E395.

Drake M. J. (1986) Is lunar bulk material similar to Earth's mantle? In Origin of the Moon (W. K. Hartmann, R. J. Phillips and G. J. Taylor, eds.), pp. 105-124. Lunar and Planetary Institute, Houston.

D'Uston C., Atteia J. L, Barat C., Chernenko A., Dolidze V., Dyatchkov A., Jourdian E., Khariukova V., Khavenson N., Kozienkov A., Kucherova R., Mitrofanov I., Moskaleva L., Niel M., Pozanenko A., Scheglov P., Surkov Yu., and Vilchinskaya A., (1989) Observation of the γ-ray emission from the martian surface by the APEX experiment. Nature, 341, 598-600.

Eldridge J. S., O'Kelley G. D., and Northcutt K. J. (1972) Abundances of primordial and cosmogonic radionuclides in Apollo 14 rocks and fines. Proc. Lunar Sci. Conf. 3rd. pp. 1651-1658.

Eldridge J. S., O'Kelley G. D., and Northcutt K. J. (1973) Radionuclide concentrations in Apollo 16 lunar samples determined by nondestructive gamma-ray spectrometry. Proc. Lunar Sci. Conf. 4th, pp. 211.5-2122.

Eldridge J. S., O'Kelley G. D., and Northcutt K. J. (1974) Primordial radioelement concentrations in rocks and soils from Taurus-Littrow. Proc. Lunar Sci. Conf. 5th, pp. 1025-1033.

Eliason E. M. and Soderblom L. A. (1977) An array processing system for lunar geochemical and geophysical data. Proc Lunar Sci. Conf. 8th, pp. 1163-1170.

Etchegaray-Ramirez M. I., Metzger A. E., Haines E. L., and Hawke B. R. (1983) Thorium concentrations in the lunar surface: IV. Deconvolution of the Mare Imbrium, Aristarchus, and adjacent regions. Proc Lunar Planet. Sci Conf. 13th, in J. Geophys. Res., 88, A529-A543.

Frontispiece (1974). Proc. Lunar Sci. Conf. 5th vol. 1. Plate 2.

Frontispiece (1976). Proc. Lunar Sci. Conf 7th vol. 1. Plate 6.

Frontispiece (1977). Proc. Lunar Sci Conf. 8th vol. 1. Plate 2.

Haines E. L. and Metzger A, E. (1980) Lunar highland crustal models based on iron concentrations: Isostasy and center-of-mass displacement. Proc. Lunar Planet, Sci . Conf. 11th pp. 689-718.

Haines E. L., Etchegaray-Ramirez M. I., and Metzger A. E. (1978) Thorium concentrations in the lunar surface: 11. Deconvolution modeling and its application to the regions of Aristarchus and Mare Smythii. Proc. Lunar Planet. Sci. Conf. 9th, pp. 2985-3013.

Barrington T. M., Marshall J. H., Arnold J. R., Peterson L. E., Trombka J. I., and Metzger A. E. (1974) The Apollo Gamma-Ray Spectrometer. Nucl. Instr. Methods, 118, 401-411.

Hartmann W. K., Phillips R. J., and Taylor G. J., eds., (1986) Origin of the Moon. Lunar and Planetary Institute, Houston. 781 pp.

Haskin L. A. and Korotev R. L. (1981) On compositional modeling of lunar highlands soils, including application to the orbiting gamma-ray experimental data. Proc. Lunar Planet. Sci. 12B, pp. 791-808.

Hawke B. R. and Head J. W. (1978) Lunar KREEP volcanism: geologic evidence for history and mode of emplacement, Proc. Lunar Planet Sci. Conf 9th, pp. 3285-3309.

Head J. W. (1976) Lunar volcanism in space and time. Rev. of Geophys. and Space Phys., 14, 265-300,

James O. B. (1980) Rocks of the early lunar crust, Proc. Lunar Planet. Sci. Conf. 11th, pp. 365-393.

Janghorbani M., Miller M. D., Ma M.-S., Chyi L.I.. and Ehmann W. D. (1973) Oxygen and other elemental abundance data for Apollo 14, 15, 16, and 17 samples. Proc. Lunar Sci. Conf. 4th, pp. 1115-1126.

Johnson J. R., Larson A. M., and Singer R. B. (preprint) Remote sensing of potential lunar resources: I. Global compositional mapping. Submitted to J. Geophys. Res.

Johnson T. V., Saunders R. S., Matson D. L., and Mosher J. A. (1977) A TiO_2 abundance map for the northern maria. Proc. Lunar Sci. Conf. 8th, pp. 1029-1036.

Kaula W. M., Schubert G., Lingenfelter R. E., Sjogren W. L., and Wollenhaupt W. R. (1972) Analysis and interpretation of lunar laser altimetry, Proc. Lunar Sci. Conf. 3rd, pp. 2189-2204.

Kaula W. M., Schubert G., Lingenfelter R. E., Sjogren W. L., and Wollenhaupt W. R. (1974) Apollo laser altimetry and inferences as to lunar structure. Proc. Lunar Sci. Conf. 5th, pp. 3049-3058.

Keith J. E., Clark R. S., and Richardson K. A. (1972) Gamma-ray measurements of Apollo 12, 14, and "15 lunar samples. Proc. Lunar Sci. Conf. 3rd, pp. 1671-1680.

Korotev R. L. (1981) Compositional trends in Apollo 16 soils. Proc. Lunar Planet. Sci. 12B, pp. 577-605.

Langseth M. G., Keihm S. J., and Peters K. (1976) Revised lunar heat-flow values. Proc. Lunar Sci. Conf. 7th, pp. 3143-3171.

Laul J. C., Hill D. W., and Schmitt R. A. (1974) Chemical studies of Apollo 16 and 17 samples. Proc. Lunar Sci. Conf. 5th, pp. 1047-1066.

LSPET (1970) Preliminary examination of lunar samples from Apollo 1.2, Science, 167, 1325-1339.

LSPET (1972) The Apollo 15 lunar samples: A preliminary description. Science, 175, 363-375.

Lucey P. G. and Hawke B. R. (1988) A remote mineralogic perspective on gabbroic units in the lunar highlands. Proc. Lunar Planet. Sci Conf. 18th, pp. 355-363.

Ma M.-S., Schmitt R. A., Taylor G. J., Warner R. D., Lange D. E., and Keil K. (1978) Chemistry and petrology of Luna 24 lithic fragments and <250 μm soils: Constraints on the origin of VLT mare basalts. In Mare Crisium: The View from Luna 24 (R. B. Merrill and J. J. Papike, eds.), pp. 569-592. Pergamon Press, New York

Metzger A. E. and Drake D. M. (1990) Identification of lunar rock types and search for polar ice by gamma ray spectroscopy J. Geophys Res., 95, 449-460.

Metzger A. E. and Parker R. E. (1979) The distribution of titanium on the lunar surface. Earth Planet. Sci. Lett., 45, 155-171.

Metzger A. E. Anderson E. C., Van Dilla, M. A. and Arnold J. R. (1964) Detection of an interstellar flux of gamma rays. Nature 204, 766-767,

Metzger A. E., Trombka J. I., Peterson L. E., Reedy R. C., and Arnold J. R. (1972) A first look at the lunar orbital gamma-ray data. Proc. Lunar Sci. Conf. 3rd, Vol. 3, Frontispiece.

Metzger A, E., Trombka J. I., Peterson L. E., Reedy R. C., and Arnold J. R. (1973) Lunar surface radioactivity: Preliminary results of the Apollo 15 and Apollo 16 gamma-ray spectrometer experiments. Science, 179, 800-803.

Metzger A. E., Trombka J. I., Reedy R. C., and Arnold J. R. (1974) Element concentrations from lunar orbital. gamma-ray measurements. Proc. Lunar Sci. Conf. 5th, pp. 1067-1078.

Metzger A. E., Haines E. L., Parker R. E., and Radocinski R. G. (1977) Thorium concentrations in the lunar surface: I. Regional values and crustal content. Proc. Lunar Sci. Conf. 8th, pp. 949-999.

Papike J. J. and Vaniman D, T. (1978) Luna 24 ferrobasalts and the mare basalt suite: Comparative chemistry, mineralogy, and petrology. In Mare Crisium: The View from Luna 24, (R. B. Merrill and J. J, Papike, eds.), pp. 371-401. Pergamon Press, New York.

Parker R. E., Haines E. L., and Metzger A. E. (1981) Potassium concentrations in the lunar surface (abstract). In Lunar and Planetary Science XII, pp. 811-182. Lunar and Planetary Institute, Houston.

Patterson J. H., Franzgrote E. J., Turkevich A. L., Anderson W. A., Economou T. E., Griffin H. E., Grotch S, L., and Sowinski K. P. (1969) Alpha scattering experiment on Surveyor 7: Comparison with Surveyors 5 and 6. J. Geophys. Res., 74, 6120-6148,

Phillips R. ed. (1986) LGO Science Workshop, Contributions of a Lunar Geoscience Observer Mission to Fundamental Questions in Lunar Science. Department of Geological Sciences, Southern Methodist University, Dallas, Tx .

Pieters C. M., Head J. W., Adams J. B., McCord T. B., Zisk S. H., and Whitford-Stark J. L. (1980) Late high-titanium basalts of the western maria: Geology of the Flamsteed region of Oceanus Procellarum. J. Geophys. Res., 85, 3913-3938,

Rancitelli L. A., Perkins R. W., Felix W. D., and Wogman N. A. (1972) Lunar surface processes and 'cosmic ray characterization from Apollo 12-15 lunar sample analyses. Proc. Lunar Sci. Conf. 3rd, pp. 1681-1691.

Reedy R. C. (1978) Planetary gamma-ray spectroscopy. Proc. Lunar Planet. Sci. Conf. 9th, pp. 2961-2984.

Reedy, R. C., Arnold J. R., and Trombka J. I. (1973) Expected gamma-ray emission from the lunar surface as a function of chemical composition. J. Geophys. Res., 78, 5847-5866.

Reedy R. C., Bielefeld M. J., Trombka J. I., Metzger A. E., and Arnold J. R, (1975) Intermare and intramare comparisons of element concentrations determined by orbital gamma-ray spectroscopy. In Origins of Mare Basalts and their Implications for Lunar Evolution, pp. 130-134. Lunar Science Institute, Houston.

Rhodes J. M., Hodges F. N., and Papike J. J. (1975) Mare basalts: Major element composition and classification. In Origins of Mare Basalts and Their Implications for Lunar Evolution, pp. 135-139. Lunar Science Institute, Houston.

Ryder G. and Taylor G. .7. (1976) Did mare-type volcanism commence early in lunar history? Proc. Lunar Sci. Conf. Zth, pp. 1741-1755.

Schonfeld E. (1974) The contamination of lunar highland rocks by KREEP: Interpretation by mixing models. Proc. Lunar Sci. Conf. 5th, pp. 1269-1286.

Schonfeld E. (1977) Comparison of orbital chemistry with crustal thickness and lunar sample chemistry. Proc. Lunar Sci. Conf. 8th, pp. 1149-1162.

Schonfeld E. and Meyer C., Jr. (1972) The abundances of components of the lunar soils by a least-squares mixing model and the formation age of KREEP . Proc. Lunar Sci. Conf., 3rd, pp. 1397-1420.

Schonfeld E. and Meyer C. , Jr. (1973) The old Imbrium hypothesis. Proc. Lunar Sci Conf. 4th, pp. 125-138.

Spudis P.D. (1978) Composition and origin of the Apennine Bench Formation. Proc. Lunar Planet. Sci. Conf. 9th, pp. 3379-3394.

Spudis P. D. and Hawke B. R, (1981) Chemical mixing model studies of lunar orbital geochemical data: Apollo 16 and 17 highlands compositions. Proc. Lunar Planet. Sci. 12B, pp. 781-789.

Spudis P. D., Hawke B. R., and Lucey P. (1984) Composition of Orientale Basin deposits and implications for the lunar basin-forming process. Proc. Lunar Planet. Sci. Conf. 15th, in J. Geophys. Res., 89, C197-C210.

Surkov Yu. A, Moskalyova L. P., Manvelyan O. S., Basilevsky A.T., and Kharyukova V. P. (1980) Geochemical interpretation of the results of measuring gamma-radiation of Mars. Proc. Lunar Planet. Sci. Conf. 11th, pp. 669-676.

Tatsumoto M., Hedge C. E., Doe B. R., and Unruh D. M. (1972) U-Th-Pb and Rb-Sr measurements on some Apollo 14 lunar samples, Proc. Lunar Sci. Conf. 3rd, pp. 1531-1555.

Taylor S. R. (1975) Lunar Science: A Post-Apollo View. Pergamon Press, New York. 372 pp.

Taylor S. R. (1982) Planetary Science: A Lunar perspective. Lunar and Planetary Institute, Houston. 481 pp.

Taylor S. R. (1986) The origin of the Moon: Geochemical considerations. In Origin of the Moon, (W. K. Hartmann, R. J. Phillips and G. J. Taylor, eds.), pp. 125-144. Lunar and Planetary Institute, Houston.

Tera F. and Wasserburg G. J. (1972a) U-Th-Pb analyses of soil from the Sea of Fertility, Earth Planet. Sci. Lett. 13, 457-466,

Tera, F. and Wasserburg G. J. (1972b) U-Th-Pb systematic in lunar highland samples from the Luna 20 and Apollo 1.6 missions. Earth Planet. Sci. Lett. 17, 36-51.

Trombka J. I., Arnold J. R., Reedy R. C., Peterson L. E., and Metzger A. E. (1973) Some correlations between measurements by the Apollo gamma-ray spectrometer and other lunar observations. Proc. Lunar Sci. Conf. 4th, pp. 2847-2853.

Trombka J. I., Arnold J. R., Adler I., Metzger A. E., and Reedy R. C. (1977) Lunar elemental analysis obtained from the Apollo gamma-ray and X-ray remote *sensing* experiment. In Soviet-American Conference on the Cosmochemistry of the Moon and Planets (J. H. Pomeroy and N, J. Hubbard, eds.), pp. 153-182. NASA Report SP 370.

Trombka J. I. and Schmadebeck R. L. (1968) A Numerical Least-squares Method for Resolving Complex Pulse Height Spectra. NASA SP-3044, 170 pp.

Trombka J. I., Schmadebeck R. L., Bielefeld M. J., Evans L. G., Metzger A. E., Haines E. L., Dyer C. S., Seltzer S. M., Reedy R. C., and Arnold J, R. (1979) Analytical methods in determining elemental composition from the Apollo X-ray and gamma-ray spectrometer data. In Computers in Activation Analysis and Gamma-Ray Spectroscopy (B. A, Carpenter, M. D'Agostino and H. Yule, eds.), DOE CONF-780421, pp. 26-38. NTIS, Springfield, Va.

Turkevich A. L. (1971) Comparison of the analytical results from the Surveyor, Apollo, and Luna missions. Proc. Lunar Sci. Conf.2nd, pp. 1209-1215.

Van Dills M. A., Anderson E. C., Metzger A. E., and Schuch R. L. (1962) Lunar composition by scintillation spectroscopy. IRE Trans. Nucl. Sci. NS-9, 405-412.

Vinogradov A. P., Surkov Yu. A., Chernov G. M., Kirnozov F. F., and Nazarkina G. B. (1968) Gamma investigation of the Moon and composition of the lunar rocks. In Moon and Planets II (A. Dollfus, cd.), pp. 77-90, North-Holland, Amsterdam.

York D. (1969) Least squares fitting of a straight line with correlated errors, Earth Planet. Sci. Lett., 5, 320-324.

Table 1. Regional Averages of Th, Fe and Ti Concentrations[a]

Location	Concentrations		
	Th (ppm)[b]	Ti (%)[c]	Fe (%)[d]
Farside highlands west	0.43 ± 0.07	0.7 ± 0.4	5.1 ± 0.9
Farside highlands east	0.66 ± 0,08	(),9 ± 0.3	5.5 ± 0.9
Limb highlands west	0.38 ± 0.07	0.5 ± 0.4	4.6 ± 0.8
Limb highlands east	0,72 ± 0.07	0.9 ± 0.4	7.9 ± 0.9
Nearside highlands west	1.24 ± 0.15	0.9 ± 0.4	6.5 ± 1.2
Nearside highlands east	1.13 ± 0.10	0.9 ± 0.4	8.2 ± 1.0
Central highlands	2.2 ± 0.2	0.7 ± 0.4	5.1 ± 1.0
Entire highlands	0.70 ± 0.06	0.8 ± 0.3	5.9 ± 0.7
Eastern maria	1.82 ± 0.15	2.1 ± 0.4	12.0 ± 1.1
Western maria	4,6 ± 0.4	2.0 ± 0.4	12.7 ± 0.8

' Area weighted

[b] From Metzger et al., 1.977a

[c] From Metzger and Parker, 1979

[d] From Davis, 1980

Table 2. Lunar Surface Model

Province	Eastern Maria	Western Maria	Central &Mare Highlands Border	Farside & non-mare Highlands border	KREEP-rich
Fractional Area (%)	4.8	10.2	24.2	59.8	1.1
[Th] ppm	1.79	4,4	1.47	0.53	7.4

Table 3. Site comparison of sample and orbital thorium concentrations in ppm by weight

	Mare Tranquillitatis (Apollo 11)	Oceanus Procellarum (Apollo 12)	Fra Mauro (Apollo 14)	Hadley (Apollo 15)	Descartes (Apollo 15)
Soil sample	2.2[a]	6.3[b]	12.6[c]	4.3[d]	1.9[e]
Orbital[f]	2.3 ± .3	5.9 ± .5	8.2 ± .6	4.2 ± .4	2.0 ± .2[g]
Track-site separation (km)	280	325	170	—	—

	Littrow (Apollo 17)	Mare Fecunditatis (Luna 16)	Highlands North of M. Fecunditatis (Luna 20)	Mare Crisium (Luna 24)
Soil sample	2.0[h]	1.2[i]	1.1[j]	0.7[k]
Orbital	1.9 ± .2	1.7 ± .2	1.1 ± .1[l]	1.4 ± .2
Track-site separation (km)	—	—	—	—

[a]LSPET (1972); Rancitelli et al. (1972)
[b]LSPET (1970); Rancitelli et al. (1972)
[c]Tatsumoto et al. (1972); Eldridge et al. (1972)
[d]Rancitelli et al. (1972); Keith et al. (1972)
[e]Eldridge et al. (1973); Korotev (1981)
[f]Metzger et al. (1977a)
[g]Deconvolved value is 1.6±.4 ppm
[h]Eldridge et al. (1974); Laul et al. (1974)
[i]Tera and Wasserburg (1972a)
[j]Tera and Wasserburg (1972b)
[k]Ma et al. (1978); Barsukov et al. (1977)
[l]From highland units only

FIGURE CAPTIONS

1. Speculation on lunar composition prior to the space age (courtesy of E.C. Anderson and M. A. Van Dills - Los Alamos Scientific Laboratory),

2. Measured lunar gamma-ray spectrum and its constituent components. The discrete line spectrum (+) containing the geochemical information remains after subtraction of the background, The energy scale is 19.3 keV/channel (Bielefeld et al., 1976),

3. Discrete line spectrum from the lunar surface (+), plus the monoelemental and monoenergetic lines with which it has been fit by the response function method. The energy scale of the abscissa is 19.3 keV/channel. The positron line is at 511 keV; the Hg-203 calibration line is at 279 keV. The top curve is the total synthesized spectrum (Bielefeld et al., 1976).

4. Profiles of the observed data field and the deconvolved model field for two latitude strips over the Aristarchus and adjacent regions. Comparison . shows the sharpening of contrast and accompanying improvement in spatial resolution resulting from deconvolution (Haines et al. , 1978). The arrows show the location of regional. boundaries.

5. Early map of lunar radioactivity in the energy region from 0.55 to 2,75 MeV over the Apollo 15 and Apollo 16 ground tracks: (A) nearside; (B) farside. The intensity key is in counts per second (Metzger et al.. , 1973) .

6. Map of the thorium concentration in the lunar regolith for the area overflown by Apollo 15 and 16, based on the 0.55-2,75 MeV gamma-ray energy band analysis of orbital data (Metzger et al., 1977a).

7. The regression curve for titanium. Ground site soil values in weight percent are plotted vs. the integrated count rate for the region which contains the site. Typical error bars are shown for the unit weighting (±1%) applied to the ordinate (Metzger and Parker, 1979).

8. Map of the titanium concentration in the lunar regolith for the area overflown by Apollo 15 and 16, based on the 5.95-6.37 MeV gamma-ray energy band analysis of orbital data (Metzger and Parker, 1979).

9. Map of the iron concentration in the lunar regolith for the area overflown by Apollo 15 and 16, based on the 6.99-8.89 MeV gamma-ray energy band analysis of orbital data (Davis, 1980).

10 The ratio of K/Th as a function of Th, categorized by major regional type . The K/Th ratio decreases asymptotically with increasing Th. Typical K/Th ratios of lunar soil samples are shown for comparison (Metzger et al., 1977a).

11. Composite deconvolution model for the Aristarchus, Imbrium, and Apenninus regions with the Th concentration range for each construct (Etchegarey-Raimirez et al., 1983).

12. Thorium concentrations vs crustal thickness for farside, limb, and nearside highland regions including the regions in and around Van de Graaff (Metzger et al., 1977a). The crustal thickness values are derived from the map by Bills and Ferrari (Frontispiece, 1976).

13. Plots of crustal density and crustal thickness vs. elevation for 33 highland regions. Trend lines are shown for the Pratt. and Airy modes of isostatic compensation (Haines and Metzger, 1980).

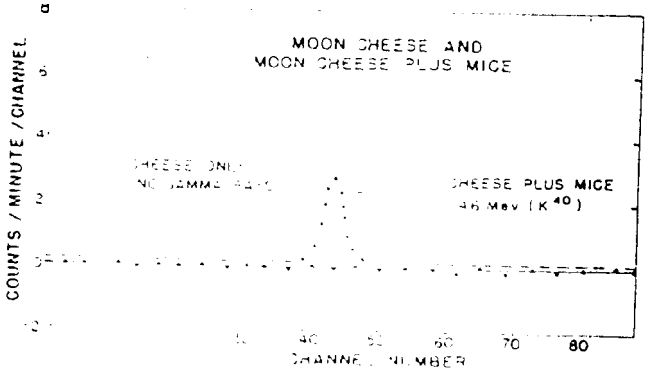
MOON CHEESE AND
MOON CHEESE PLUS MICE
CHEESE PLUS MICE
1.46 Mev (K40)
COUNTS / MINUTE / CHANNEL
CHANNEL NUMBER

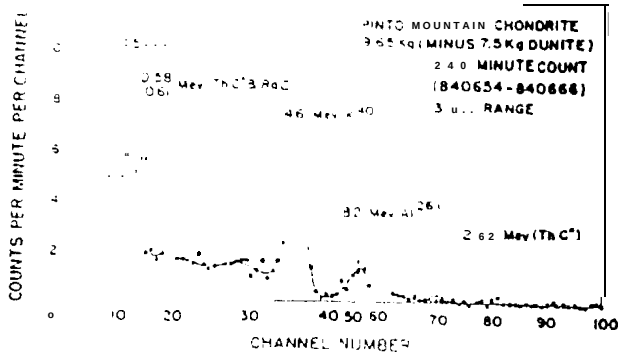
PINTO MOUNTAIN CHONDRITE
3.65 Kg (MINUS 7.5 Kg DUNITE)
240 MINUTE COUNT
(840654-840666)
3 g/cm² RANGE
0.58 Mev ThC"β RaC
1.46 Mev K40
1.82 Mev Al26
2.62 Mev (ThC")
COUNTS PER MINUTE PER CHANNEL
CHANNEL NUMBER

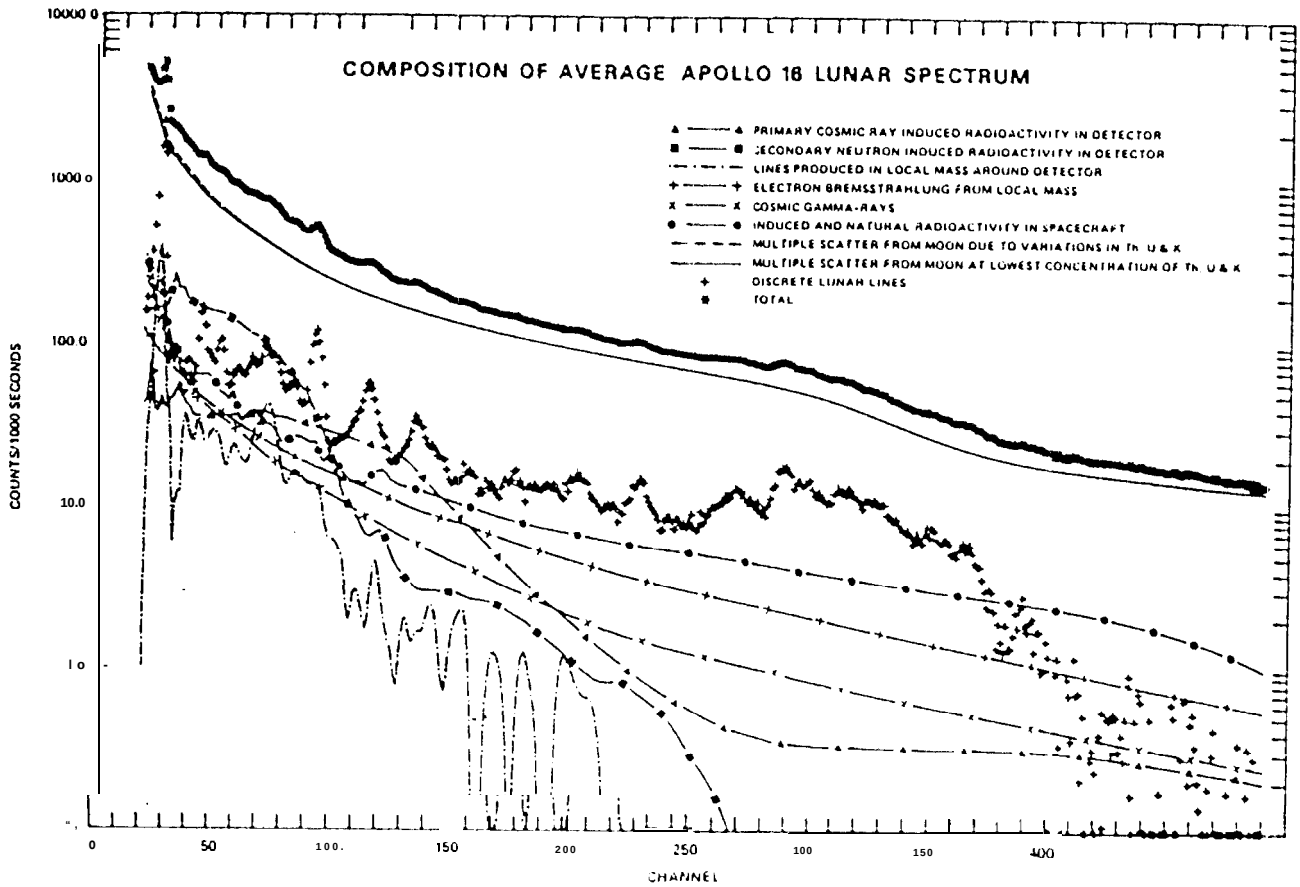
COMPOSITION OF AVERAGE APOLLO 16 LUNAR SPECTRUM
PRIMARY COSMIC RAY INDUCED RADIOACTIVITY IN DETECTOR
SECONDARY NEUTRON INDUCED RADIOACTIVITY IN DETECTOR
LINES PRODUCED IN LOCAL MASS AROUND DETECTOR
ELECTRON BREMSSTRAHLUNG FROM LOCAL MASS
COSMIC GAMMA-RAYS
INDUCED AND NATURAL RADIOACTIVITY IN SPACECRAFT
MULTIPLE SCATTER FROM MOON DUE TO VARIATIONS IN Th U & K
MULTIPLE SCATTER FROM MOON AT LOWEST CONCENTRATION OF Th U & K
DISCRETE LUNAR LINES
TOTAL
COUNTS/1000 SECONDS
10000 0
1000 o
100 0
10.0
1 o
0
50
100.
150
200
250
100
150
400
CHANNEL

FIGURE 2

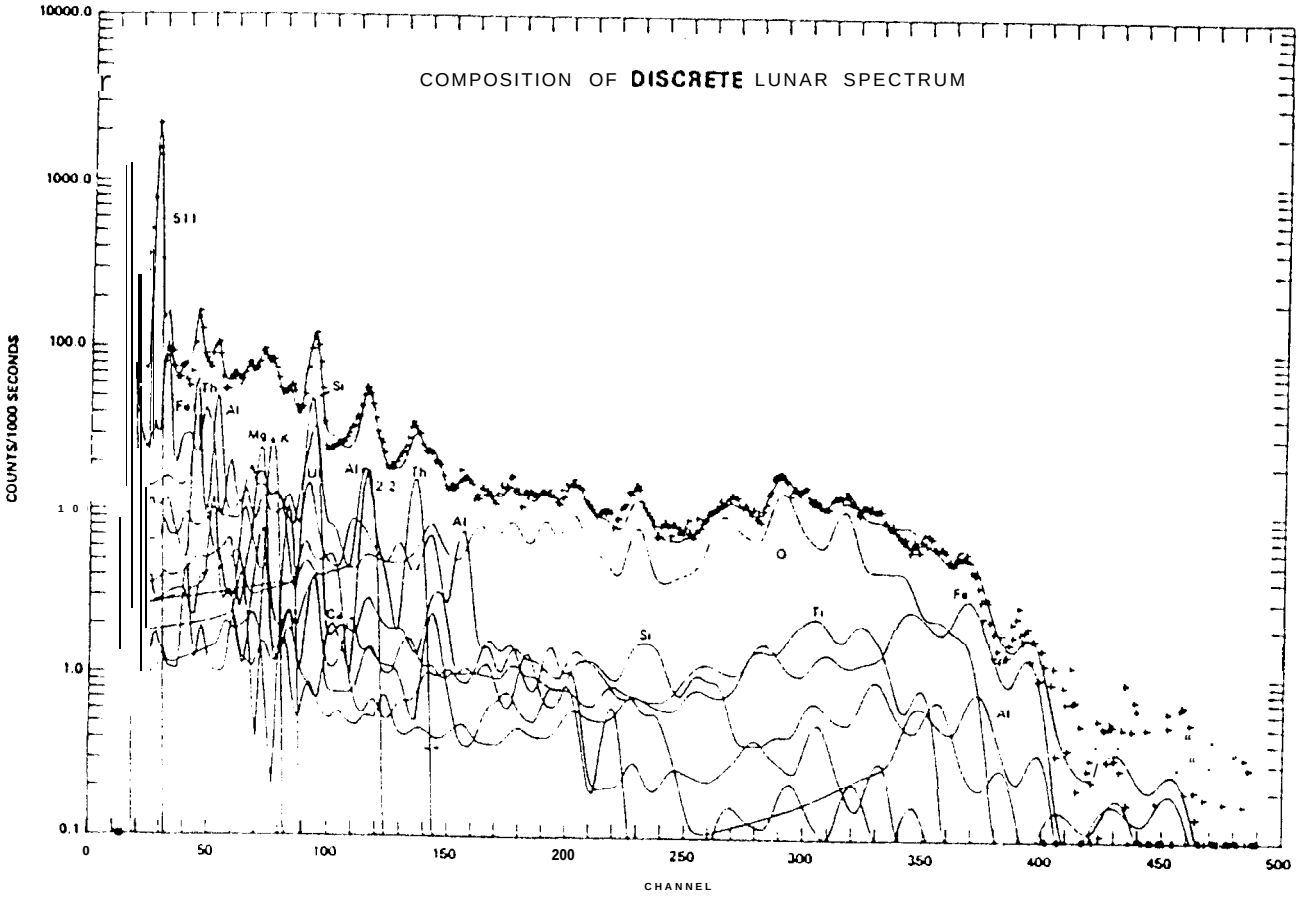
COMPOSITION OF DISCRETE LUNAR SPECTRUM
COUNTS/1000 SECONDS
10000.0
1000.0
100.0
1.0
0.1
CHANNEL
0
50
100
150
200
250
300
350
400
450
500
Si
Th
Fe
Al
Mg
K
Ca
O
Ti

FIGURE 3

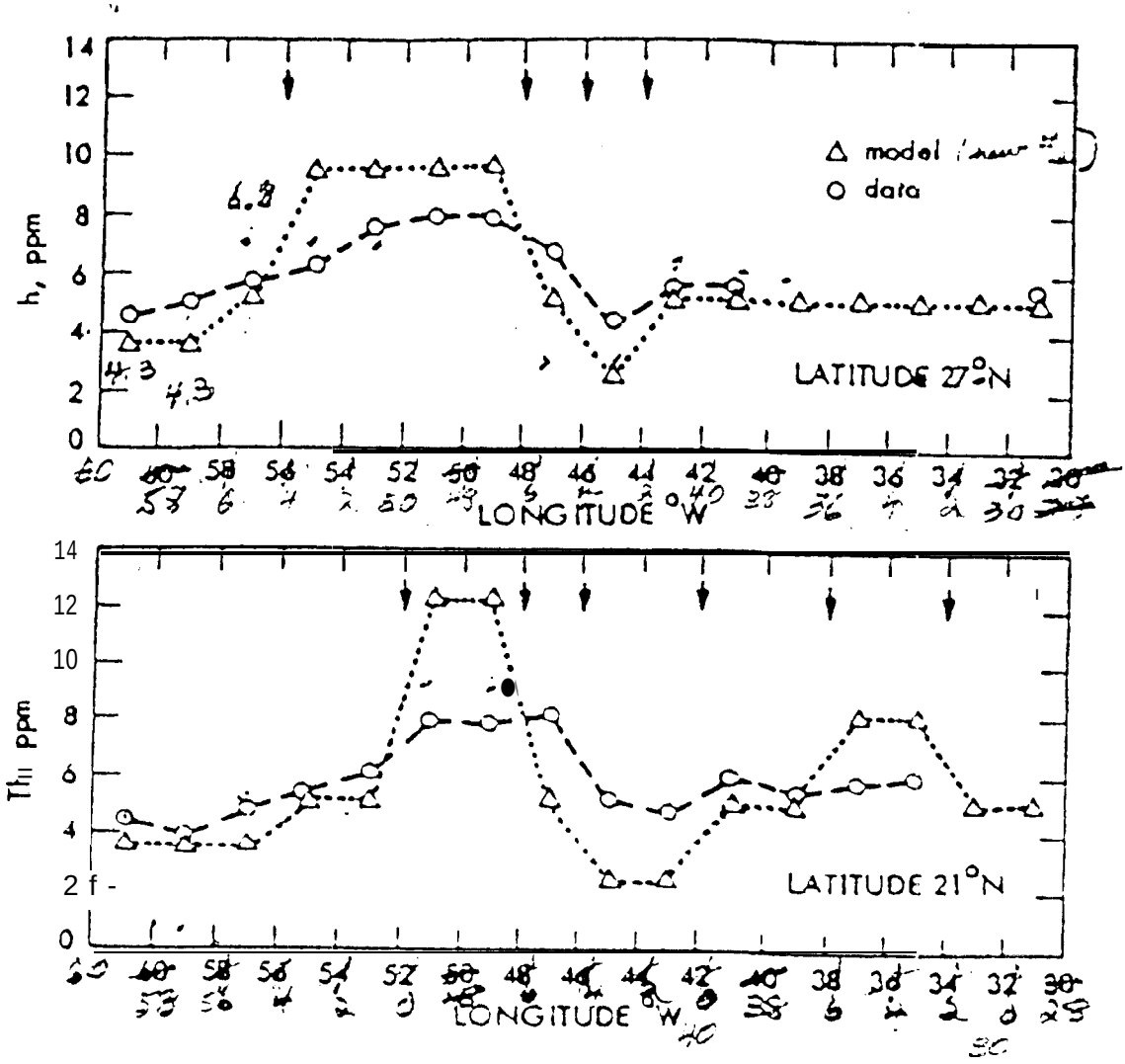
14
12
10
8
6
4
2
0
h, ppm
△ model
○ data
LATITUDE 27°N
LONGITUDE °W
14
12
10
8
6
4
2
0
Th, ppm
LATITUDE 21°N
LONGITUDE W

FIGURE 4

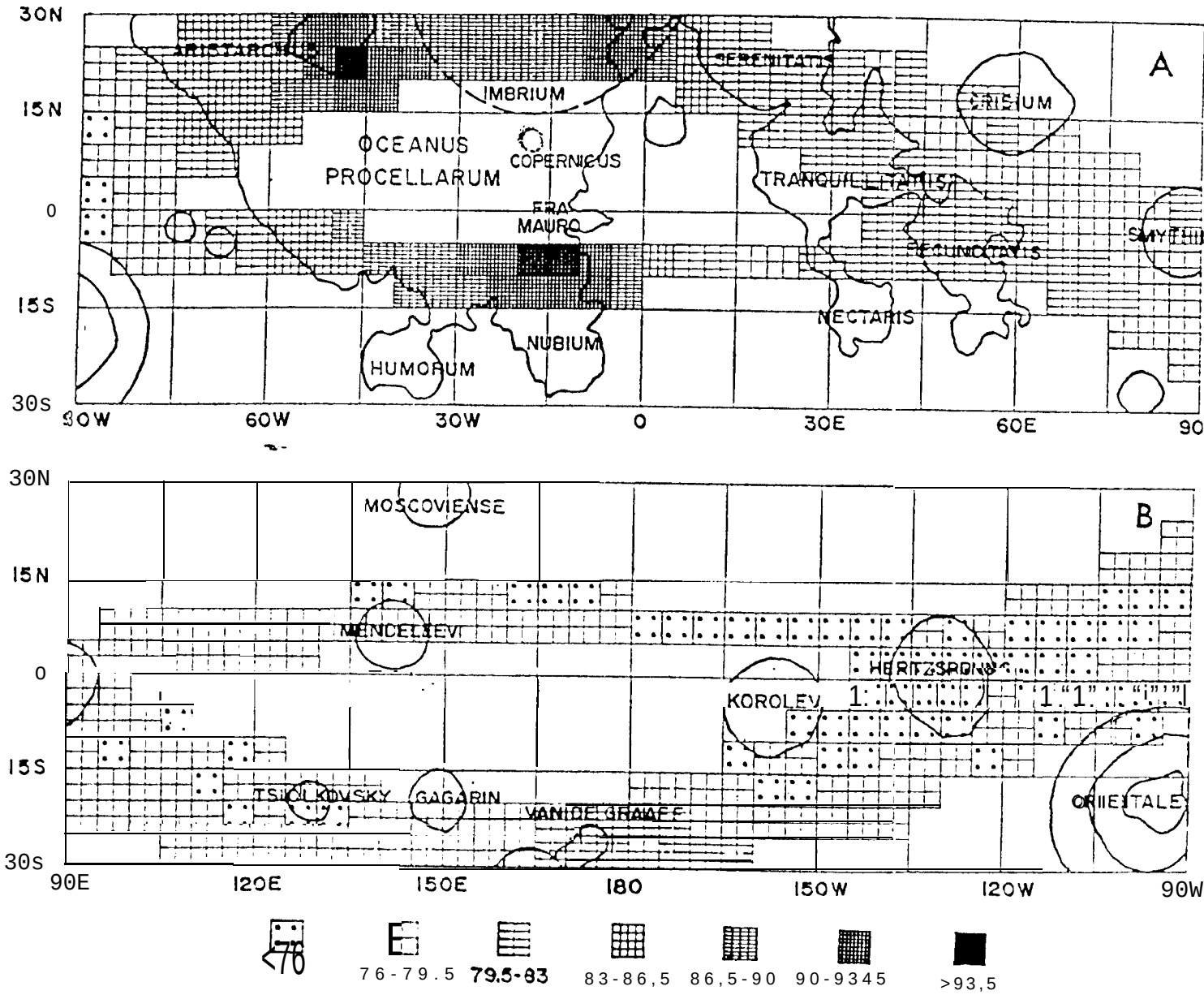
30N
15N
0
15S
30s
ARISTARCHUS
IMBRIUM
SERENITATIS
A
OCEANUS
PROCELLARUM
COPERNICUS
TRANQUILLITATIS
FRA
MAURO
NECTARIS
NUBIUM
HUMORUM
60W
30W
0
30E
60E
MOSCOVIENSE
B
MENDELEEV
KOROLEV
TSIOLKOVSKY
GAGARIN
VANDE GRAAFF
90E
120E
150E
180
150W
120W
90W
<70
76-79.5
79.5-83
83-86,5
86,5-90
90-9345
>93,5

FIGURE 5

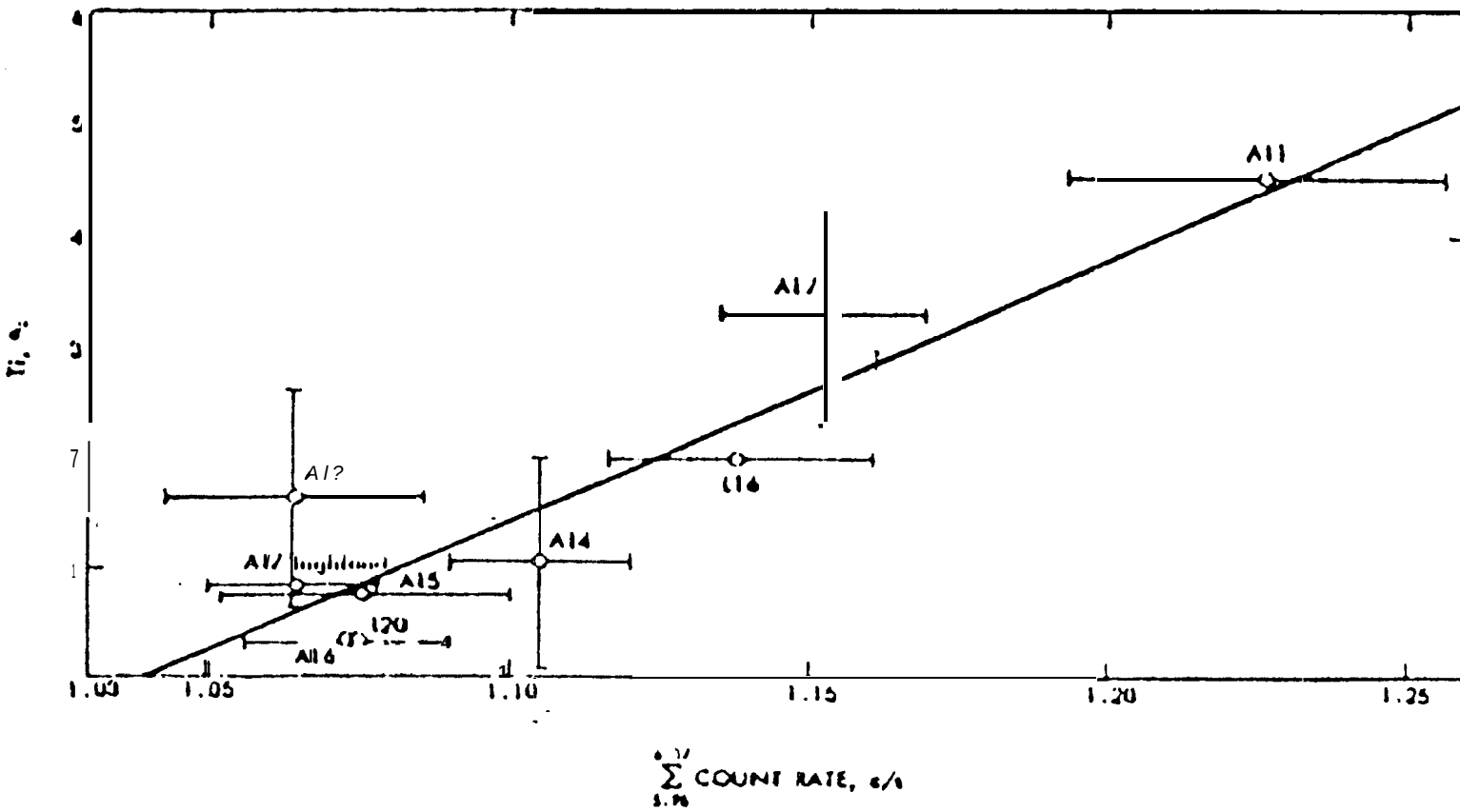

FIGURE 7

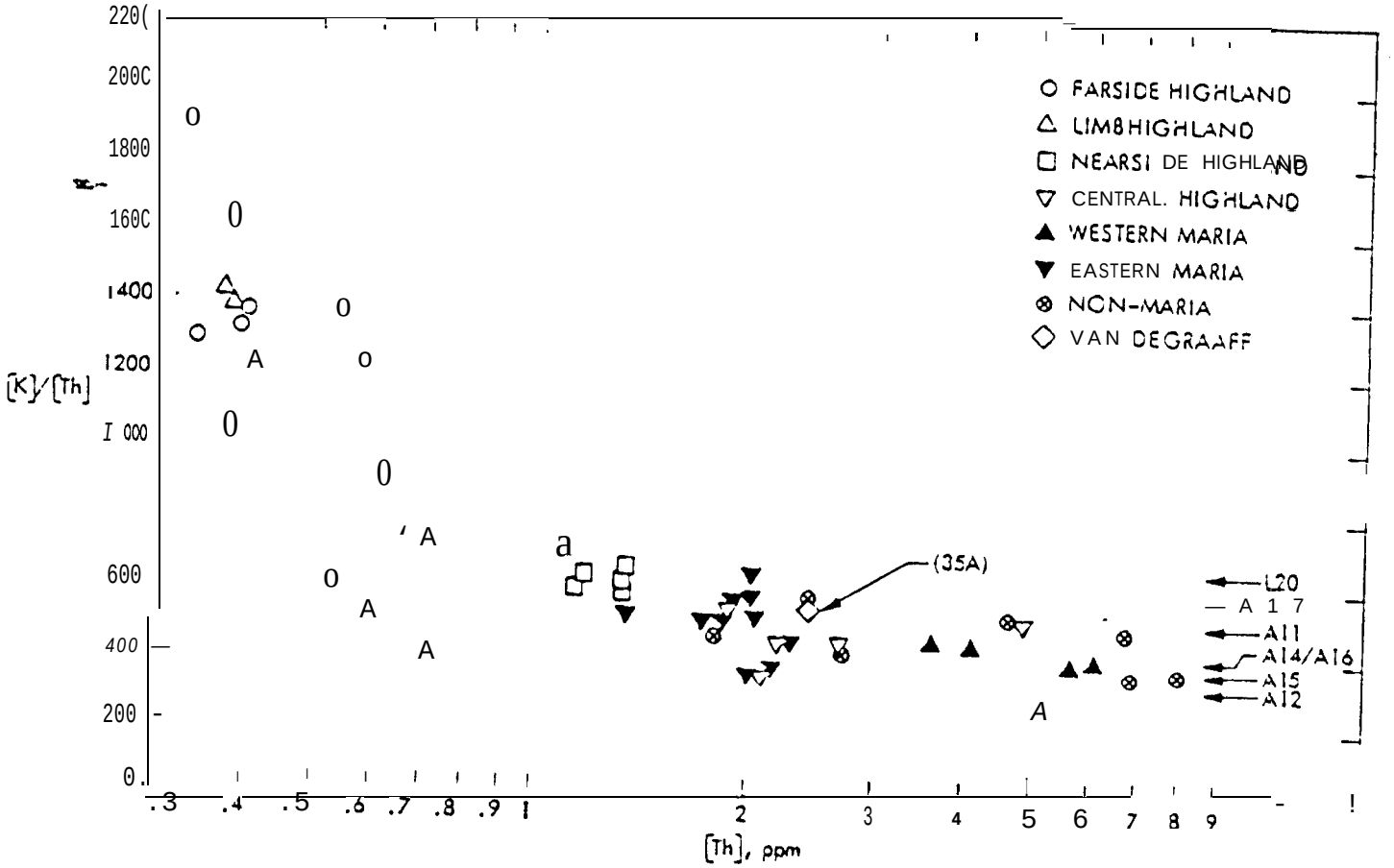
FARSIDE HIGHLAND
LIMB HIGHLAND
NEARSIDE HIGHLAND
CENTRAL HIGHLAND
WESTERN MARIA
EASTERN MARIA
NON-MARIA
VAN DEGRAAFF
[K]/[Th]
[Th], ppm
(35A)
L20
A17
A11
A14/A16
A15
A12

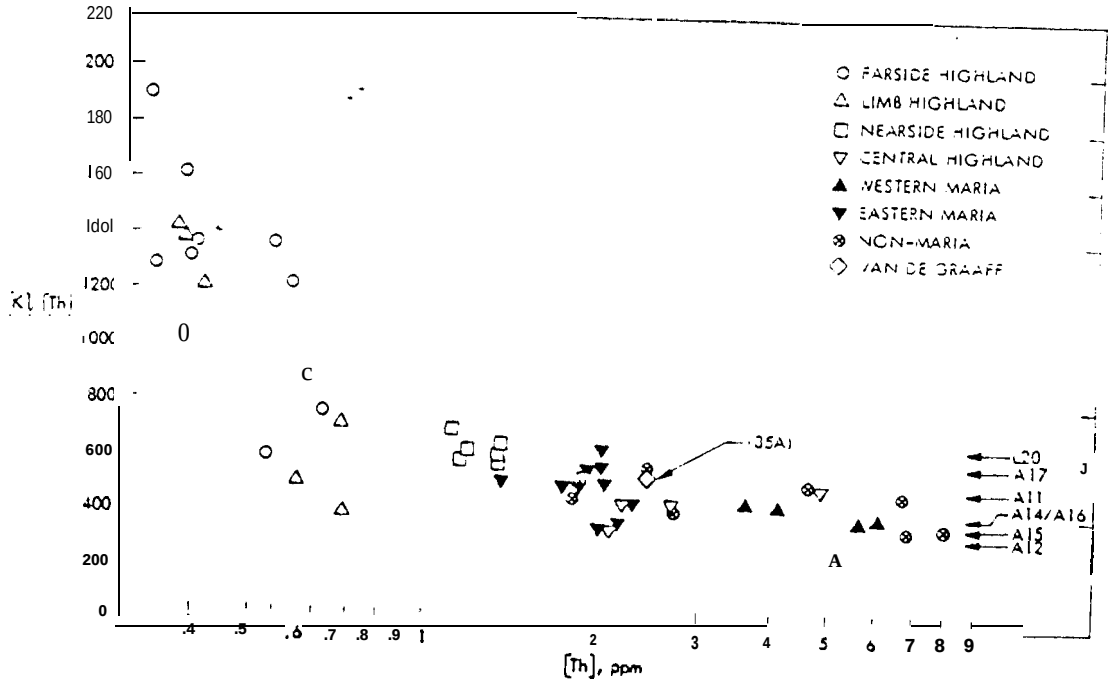
FARSIDE HIGHLAND
LIMB HIGHLAND
NEARSIDE HIGHLAND
CENTRAL HIGHLAND
WESTERN MARIA
EASTERN MARIA
NON-MARIA
VAN DE GRAAFF
[Th], ppm
(35A)
L20
A17
A11
A14/A16
A15
A12

FIGURE 10

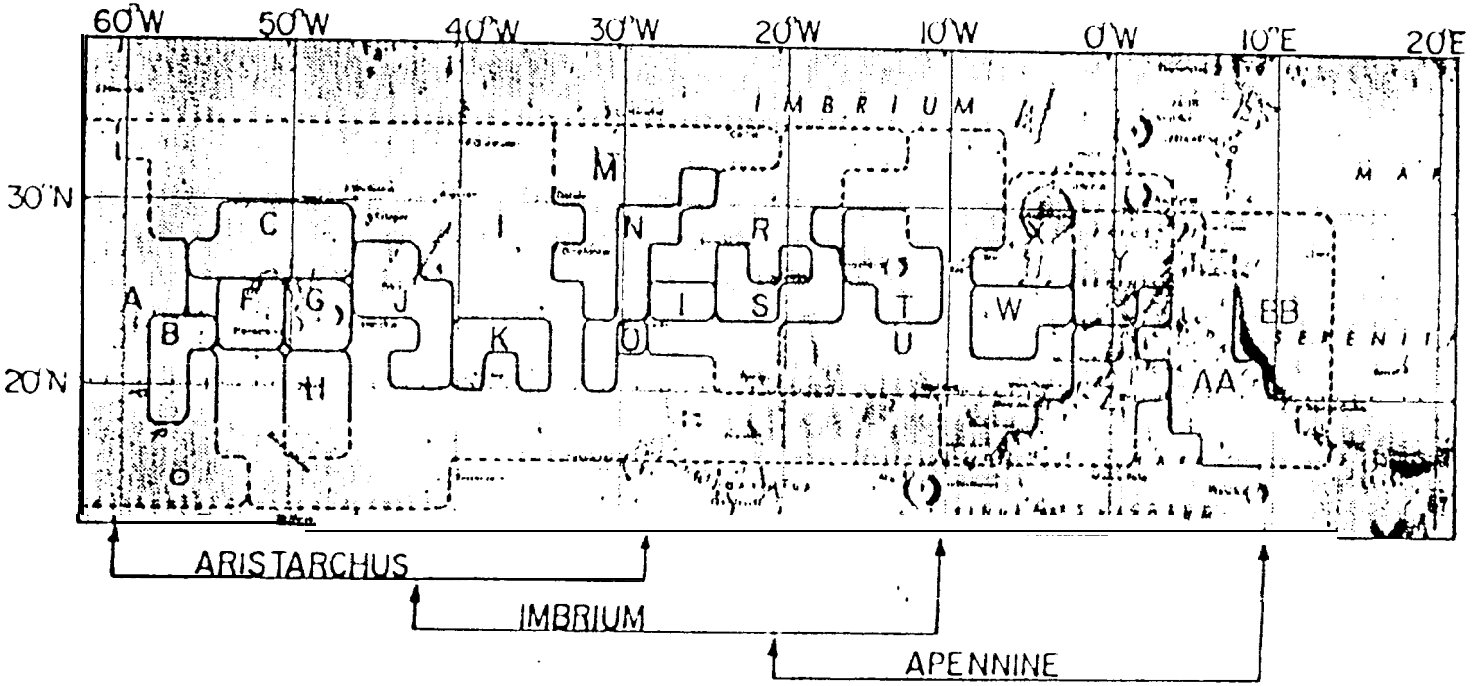
60°W
50°W
40°W
30°W
20°W
10°W
0°W
10°E
20°E
30°N
20°N
IMBRIUM
A
B
C
F
G
H
I
J
K
M
N
O
R
S
T
U
W
BB
AA
ARISTARCHUS
IMBRIUM
APENNINE

FIGURE 11

Legend for Figure 11

	Construct	Long (°W)	Concentration
A.	W. Procellarum	52-66	4.3(0.3)
B.	'Low' Th	54-58	O- 0.8(1.9)
C.	Aristarchus N. Plateau	46-56	7.8- 8.2(0.6)
D.	Plateau northwest	46-52	6.8(1.1)
E.	Plateau northeast	52-56	9.3(1.3)
F.	Aristarchus S. Plateau	50-54	4.5- 5.3(2.0)
G.	Aristarchus Crater	46-50	18.2-21.7(2.7)
H.	Marius	46-50	8.1- 8.7(1.0)
I.	E. Procellarum	28-58	5.3- 5.5(0.4)
J.	Prinz	40-46	1.6- 2.9(1.1)
K.	Brayley	32-40	9.2-10.6(1.3)
L.	Marius & Brayley	---	7.9- 8.8(0.9)
M.	W. Imbrium	20-34	3.0- 3.4(0.5)
N.	Phase III	29	9.2-12.1(1.7)
O.	Euler	29	5.6- 9.1(3.0)
P.	Phase III & Euler	---	6.8- 8.8(1.8)
Q.	La Hire	29	10.7-11.4(1.5)
R.	Eratosthenian Mare	12-34	1.4- 1.9(0.8)
S.	Lambert	21	9.9-12.4(2.1)
T.	Timocharis	13	9.5- 9.7(1.6)
U.	E. Imbrium	8-20	3.4- 3.6(0.5)
V.	Timocharis + Lambert	---	9.3- 9.9(1.4)
W.	Apennine Bench	8- 2	10.7-12.0(2.3)
X.	Archimedes	8-4E	15.2-20 (2.5)
Y.	Palus Putredinis	2-4E	0.2- 1.7(1.4)
Z.	Apennine Mountains	6-4E	7.3- 8.2(1.0)
AA*	Haemus Mountains	2E-14E	2.9- 3.3(0.6)
BB.	Mare Serenitatis	6E-14E	1.8- 2.0(0.5)

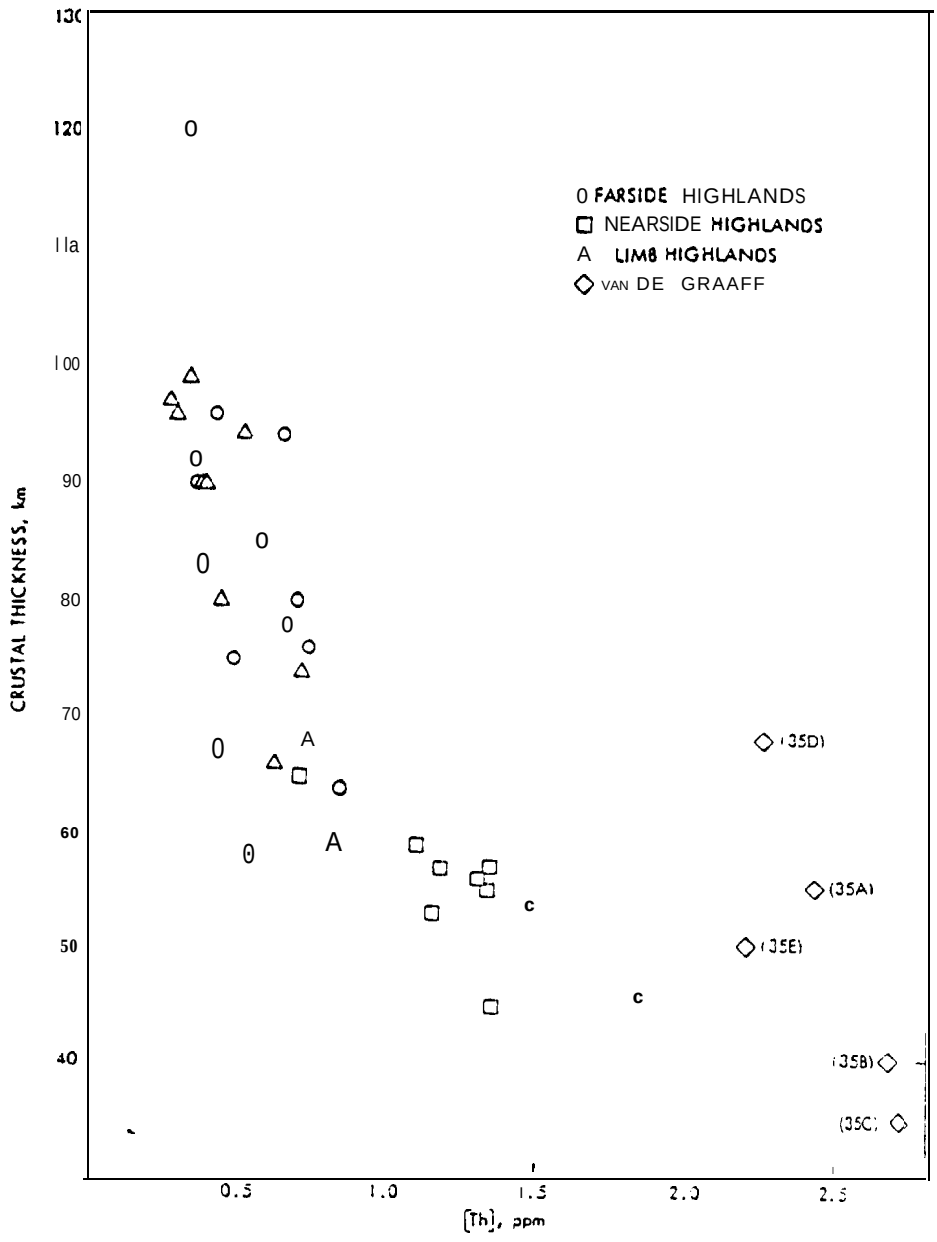
130
120
110
100
90
80
70
60
50
40
CRUSTAL THICKNESS, km
0 FARSIDE HIGHLANDS
□ NEARSIDE HIGHLANDS
A LIMB HIGHLANDS
◇ VAN DE GRAAFF
(35D)
(35A)
(35E)
(35B)
(35C)
0.5
1.0
1.5
2.0
2.5
[Th], ppm

FIGURE 12

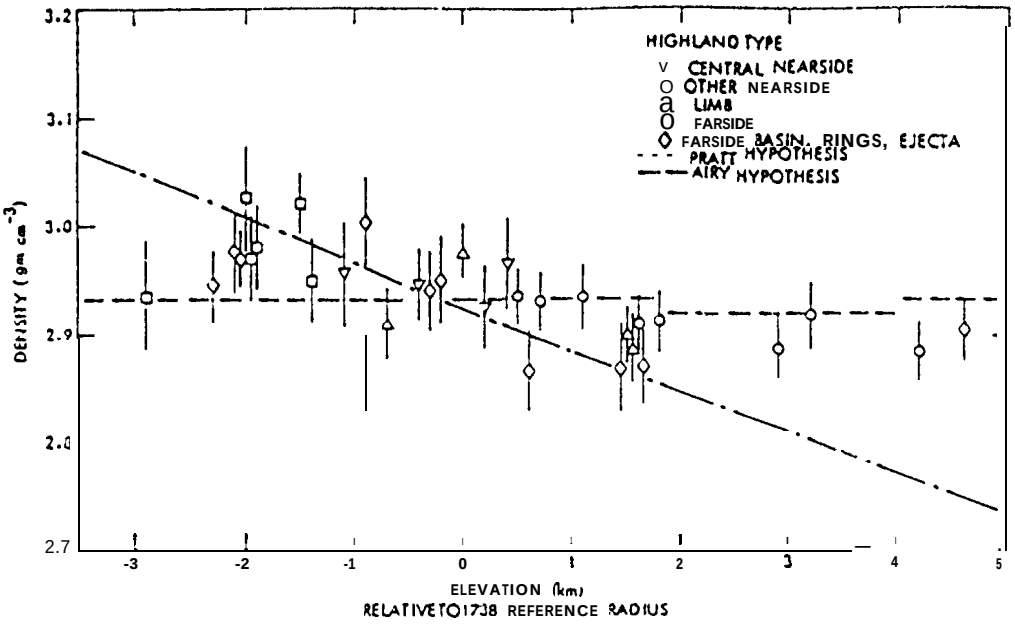
HIGHLAND TYPE
V CENTRAL NEARSIDE
O OTHER NEARSIDE
a LIMB
O FARSIDE
◊ FARSIDE BASIN, RINGS, EJECTA
PRATT HYPOTHESIS
AIRY HYPOTHESIS
DENSITY (gm cm⁻³)
3.2
3.1
3.0
2.9
2.8
2.7
-3
-2
-1
0
1
2
3
4
5
ELEVATION (km)
RELATIVE TO 1738 REFERENCE RADIUS

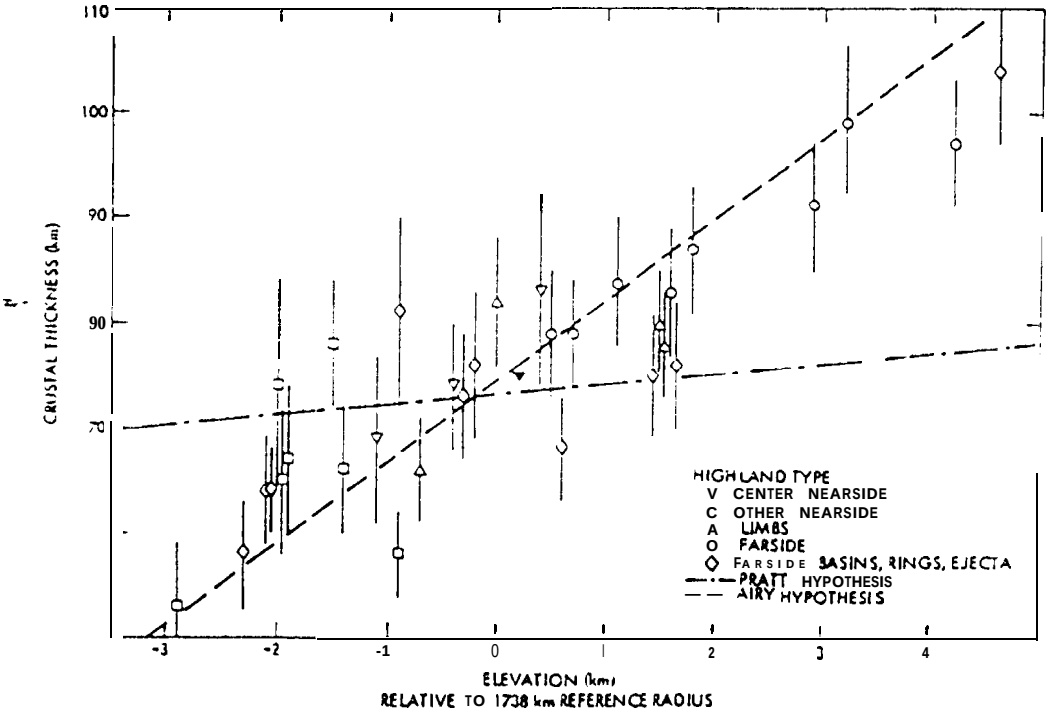
110
100
90
90
CRUSTAL THICKNESS (km)
HIGHLAND TYPE
V CENTER NEARSIDE
C OTHER NEARSIDE
A LIMBS
O FARSIDE
◊ FARSIDE BASINS, RINGS, EJECTA
PRATT HYPOTHESIS
AIRY HYPOTHESIS
-3
-2
-1
0
1
2
3
4
ELEVATION (km)
RELATIVE TO 1738 km REFERENCE RADIUS

FIGURE 13